



Review

A Review on the Processing of Aero-Turbine Blade Using 3D Print Techniques

Ayush Sinha ¹, Biswajit Swain ¹, Asit Behera ^{2,*}, Priyabrata Mallick ¹, Saswat Kumar Samal ¹,
H. M. Vishwanatha ³ and Ajit Behera ^{1,*}

¹ Department of Metallurgical and Materials Engineering, National Institute of Technology, Rourkela 769008, India; ayushaca6@gmail.com (A.S.); enggbiswajit92@gmail.com (B.S.); mallickx@gmail.com (P.M.); samalsaswat78952@gmail.com (S.K.S.)

² School of Mechanical Engineering, Kalinga Institute of Industrial Technology, Bhubaneswar 751024, India

³ Department of Mechanical and Manufacturing Engineering, Manipal Institute of Technology-Manipal, Manipal Academy of Higher Education, Manipal 576104, India; vishuhm@gmail.com

* Correspondence: asit.beherafme@kiit.ac.in (A.B.); beheraajit@nitrrkl.ac.in or ajit.behera88@gmail.com (A.B.)

Abstract: Additive manufacturing (AM) has proven to be the preferred process over traditional processes in a wide range of industries. This review article focused on the progressive development of aero-turbine blades from conventional manufacturing processes to the additive manufacturing process. AM is known as a 3D printing process involving rapid prototyping and a layer-by-layer construction process that can develop a turbine blade with a wide variety of options to modify the turbine blade design and reduce the cost and weight compared to the conventional production mode. This article describes various AM techniques suitable for manufacturing high-temperature turbine blades such as selective laser melting, selective laser sintering, electron beam melting, laser engineering net shaping, and electron beam free form fabrication. The associated parameters of AM such as particle size and shape, powder bed density, residual stresses, porosity, and roughness are discussed here.

Keywords: additive manufacturing (AM); turbine blade; designing; selective laser melting (SLM); selective laser sintering (SLS); electron beam melting (EBM); porosity; density; residual stress; roughness



Citation: Sinha, A.; Swain, B.; Behera, A.; Mallick, P.; Samal, S.K.; Vishwanatha, H. M.; Behera, A. A Review on the Processing of Aero-Turbine Blade Using 3D Print Techniques. *J. Manuf. Mater. Process.* **2022**, *6*, 16. <https://doi.org/10.3390/jmmp6010016>

Academic Editor: Steven Y. Liang

Received: 20 December 2021

Accepted: 17 January 2022

Published: 21 January 2022

Publisher's Note: MDPI stays neutral with regard to jurisdictional claims in published maps and institutional affiliations.



Copyright: © 2022 by the authors. Licensee MDPI, Basel, Switzerland. This article is an open access article distributed under the terms and conditions of the Creative Commons Attribution (CC BY) license (<https://creativecommons.org/licenses/by/4.0/>).

1. Introduction

A turbine blade is a discrete component of a gas or steam turbine engine. A series of aerofoil shaped blades are inserted in a slot of a disc that is mounted on a rotating shaft. The aerofoil shaped blades are designed to provide sufficient space between the adjacent blades so result in steady acceleration of the flow of fluid. These blades extract heat from the high temperature and high-pressure fluid flowing in between the blades. The turbine engines operate at very high temperatures of about 850–1700 °C [1], which are above the melting point of many materials. On the other hand, the housing of the turbine is subjected to a huge amount of vibrations, centrifugal forces, stresses, oxidation, and corrosion at high temperature. Such prevailing extreme conditions inside the turbine engine during operation are important parameters for the selection of materials. Hence, gas turbine blades are manufactured using exotic and expensive materials such as precipitation hardened Ni-based super alloys that can best fit for high-temperature applications. These super alloys develop strength at high temperatures due to the precipitation of hard phases. Considering all metallurgical factors, researchers and manufacturers are looking for efficient and profitable turbine manufacturing. Hence in the case of gas turbine engines, the design and manufacture turbine blades is a crucial activity. In conventional manufacturing techniques, the buy-to-fly ratio is about 20:1 [2]. For example, if one ton (1000 kg) of material is used in production, only 50 kg ends up in the final part. As the quality control

around the turbine blades is very stringent, the remaining materials require reprocessing and recycling. The production of these blades is also a complex process and is traditionally performed with two main manufacturing techniques: precision investment casting and precision machining. The investment casting (IC) technique begins with pattern making, followed by shell making, dewaxing and pouring, knockout, heat treatment, and the finished preformed part. The required patterns are made from wax. The shell making involves applying and drying several layers of material followed by dewaxing and shell burning. Hence, currently, the IC process is a slow process that consumes around 70 h, depending on the size, quality, quantity, and material of the component. Meanwhile, the precision machining manufacturing technique achieves the final geometry by machining operations to fit the shape. Final parts require chemical cleaning to detect abnormalities and defects in fabricated parts. Currently, IC can fabricate parts with superior surface finish, dimensional accuracy, and shape complexity. In addition, the aerofoil shape production requires multiple machining and precise machining, which adds to the production costs. The shape of these blades is crucial to the engine's performance, making the control on design a critical step in the entire process. As the demand for energy increases, the high-performance turbine blades consists of complex, high-tech designs that should be robust and powerful; resistant and reliable even at temperatures beyond the melting point. Thus there is a need for newer production techniques to make efficient turbine blades. In this regard, several manufacturers have explored additive manufacturing as an alternate choice to conventional techniques to tackle these issues and produce better-performing and more sustainable turbine blades.

Additive manufacturing (AM) is a technology of transforming a 3D CAD model to a physical one directly by successive addition of the required material in a layer-by-layer manner. Initially, the technology was aimed at making prototypes of the design as quick as possible and was known as rapid prototyping (RP). Eventually, the scope of RP extended to tooling as well as the manufacturing of parts and products. Today, AM has become an integral part and an important contributor to Industrial Revolution 4.0. The fabrication of functional prototype can sometimes take up to several months as engineers have to design and produce tooling such as molds. This can be reduced by considering AM, where the processing time can be reduced to more than 50%. The best example would be the development of turbine blades at Siemens in 2017 [3]. By incorporating 3D printing to develop and test functional prototypes of gas turbine blades, the development and validation time for the component was significantly reduced from two years to just two months. The other key benefits of AM that make it a choice of manufacturing in the case of critical applications are the design freedom of AM, reduced wastage of material compared to subtractive manufacturing, and significant weight reduction in the parts by the application of principles of 'Design For Additive Manufacturing' (DFAM). Such contributions are essential for aerospace applications. Through the application of DFAM principles, part consolidation can be achieved. Such parts are made in solitary constructions by the consolidation of structural and functional parts. Incorporating parts in this way reduces the number of hurdles in assembling these complicated designs. Some of the literature [4] has shown this result in a report in which 855 single parts were combined into 12 parts. As a result, it significantly reduced the weight by 45 kg, a 20% improvement in fuel consumption, resulting in a 10% increase in power output, greatly simplifying engine maintenance. The reduction in material waste was ensured by the application of DFAM and this exact material waste reduction promoted the decrease in cost production [5]. As a consequence, there has been a shift toward additive manufacturing for the production of complex engine parts and components including turbine blades. The overall ease in assembly simplifies the maintenance of these engines, leading to benefits associated with the higher availability of spare parts. AM allows for the design of different types of inbuilt cooling ducts or parts inside the turbine blade. Figure 1 shows various types of AM processed turbine blades as the design approach is incompatible with many conventional manufacturing techniques due to the constraints for producing the optimized design.

The main purpose of this review is to provide information on the various additive manufacturing processes that can enable the manufacture of turbine blades. The effect of operating parameters of various AM processes on the properties of the turbine blade has been discussed.

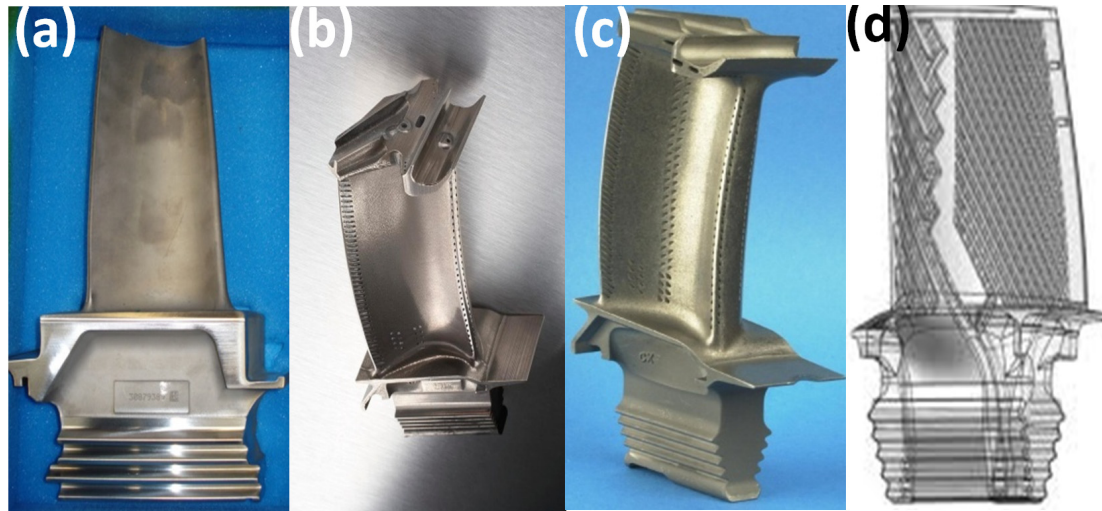


Figure 1. Various additive manufactured turbine blades. (a) Blade with the cooling passage at the edge, (b) blade with the cooling passage at both edge and middle part, (c) high-pressure turbine (HPT) blade [6], and (d) complex efficient cooling blade [7].

2. Current Scenario of Turbine Blade

The turbine blade market, being dominated by the aerospace sectors, is expected to grow at a decent pace over the next few years. The AM field is estimated to grow from \$16 billion to \$40.83 billion by 2024 [8] and in a decade, it is expected to reach \$80 billion [9], with the aerospace industry contributing significantly to this growth. Aerospace industries are adopting AM technology for prototyping, testing, and also end-use parts. The aerospace industry accounts for over 12.3% of world AM production. The thirst for high strength-to-weight ratio materials and durable materials never ends for aerospace industries. 3D printing is enhancing prototyping, production as well as the maintenance of turbine blades. Currently, the materials used to manufacture turbine blades are high melting temperature alloys, which are difficult to cast and machine. Therefore, the ability to process higher temperature alloys such as Ni-based, Co-based alloys, and intermetallic materials with flexibility is a desirable characteristic of AM. The ability to produce complex components with these materials can incorporate complex designs. Furthermore, the current construction time of monocrystalline structures can vary from 60 to 90 weeks [10]. Therefore, the reduction in production time can decrease the cost of production and increase productivity.

Engine blades are classified into three types: compressor blades, turbine blades, and fan blades used for commercial, military, and general aviation applications [11,12]. The growing demand for new generations of aircraft requires an increase in blade production as the aging fleets are being replaced every day. Demand is increasing as passenger air traffic around the world forces airlines to evolve to maintain profitability. According to Boeing, more than 17,000 aircraft are expected to be delivered over the next two years. Additionally, increased military funding is helping military aircraft developments around the world gain a head start. The Boeing 777X and Comac C919 are powered by General Electric's GE9X. The developed engine has 3D printed low-pressure (LPT) turbine blades. Leading companies in the aircraft blade market are General Electrical Company, MTU Aero Engines AG, Collins Aerospace, and Safran SA. The advancement of lightweight blades and fan structures supports the growing market. The general geography centered on the AM blade includes North America, Europe, Asia-Pacific, Latin America, the Middle East,

and Africa [13]. Figure 2 shows the percentage of global demand for aeronautical turbine blades in the commercial, military, and general aviation sectors.

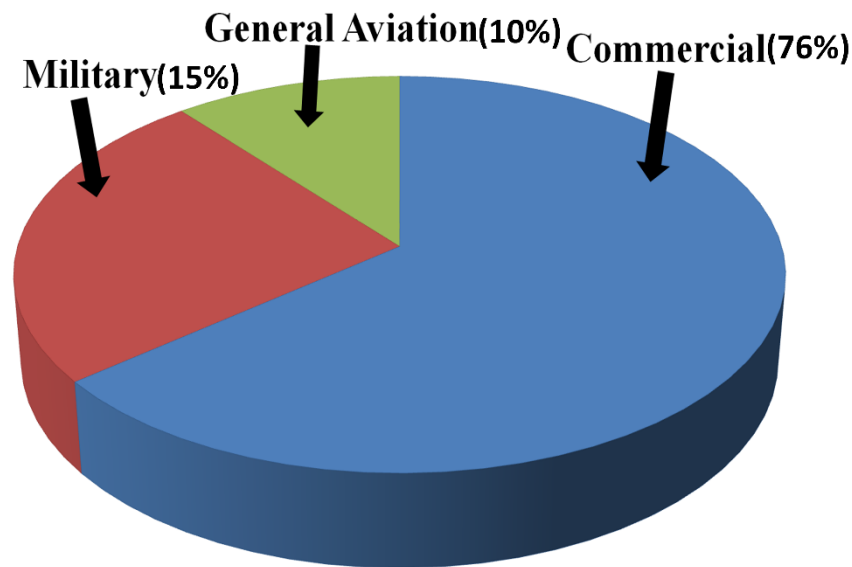


Figure 2. Aircraft engine market size in 2019 for turbine blade [14].

3. Design Development of Turbine Blade from Traditional to 3D Print Mode

Turbine blade design plays a vital role in achieving maximum efficiency of the gas turbine. Several factors affect the performance of the turbine. Since the operating temperatures are very high in the gas turbine engine, material selection is a crucial step. The metallurgical factors such as composition, structure, and property of the materials for turbine blades fall into one group. In the other group is the structure of the blade that can facilitate efficient cooling of turbine blades. The Conway engine marks the first application of the blade cooling concept that allowed designers to remove the parameter of the metal melting point as a constraint factor. As a result, the blades were able to operate at a higher turbine entry temperature (TET), thereby improving the thrust and efficiency of the gas turbine. The summary of the significant amount of literature on the evolution of turbine blade design that is focused on improving the performance of the turbine blade is presented in Table 1. The earlier generation turbine blades were operated at temperatures of 820 °C. Later, with the advent of technology and materials, newer blades could operate at 1370 °C. In the modern era, with the implementation of advanced materials, design, and processing, current turbine blades such as Snecma M88, a military aircraft, operate at 1590 °C [15]. Gas turbine blades operate in complex high pressure and temperature environments resulting in high rotational speeds. Resonating vibrations and high stresses are generated due to the high centrifugal forces of fluid. The extreme design conditions imply the high risk of failure of the blades [16]. The environment increases the susceptibility of creep failure, corrosion, and fatigue due to the presence of turbine vibrations in the engine. The architecture of the material helps to improve engine performance. Complex cooling systems (CS) can help improve blade heat management and improve engine TET. Furthermore, the production of these complex cooling systems is a major challenge using the conventional processing techniques [17].

During the 1940s, the development in the field of super-alloys and the invention of new processing methods such as vacuum induction melting contributed significantly in enhancing thermal load capacity of turbine blades. Later, during the 1950s, methods such as hot isostatic pressing were popular methods of processing turbine blades. As a result, one could see the improvement in the microstructure and performance of super-alloys. Today, high-efficiency modern engines generally use Ni-based super-alloys that contain chromium, cobalt, and rhenium. In addition, the ability to produce directionally

solidified (DS) and single crystal (SC) is a breakthrough in this field. Such processes and the resultant microstructures greatly improved the fatigue and creep resistance while eliminating grain boundaries by aligning them in one direction, hence resulting in a single crystalline structure. Single crystal research began with Pratt and Whitney. The hard work of about ten years of development was implemented in J58 engines. These J58 engines of the legendary SR-71 “Blackbird” were among the first implementations of DS technology [18]. Following the discoveries of DS and SC, thermal barrier coating (TBC) technology was another milestone in the development of turbine blades. The TBC shielded the substrate material from corrosion and oxidation, which are crucial factors at higher temperatures. In 1970, these initially experimented TBC were used in engines as aluminide coatings. In the 1980s, ceramic coatings with improved properties were implemented. The temperature capability of the turbine was improved by 90 °C during the application of coatings and in some cases, the life of the blade improved two-fold [19]. When the pressure ratio was constant in the engine, the efficiency of the engine increased. However, damage to the blades at higher operating temperatures by centrifugal forces weakened the blade, alerting to the need for the cooling of the turbine blade during operation. With the thermal barrier liner in place, passing air or liquids through the blade cavity is a good technique for cooling the blade. The higher specific heat of liquids makes them an attractive candidate for cooling application, but there is a risk of problems such as leaks, corrosion, and choking, which are the limitations of the approach. Conversely, air cooling allows for airflow to and from the chambers easily without the risk of choking. This technique allows the blade surface temperature to decrease by 200–300 °C with the help of about 1–3% of the air passing through the engine. Various techniques such as convection, film, transpiration cooling, cooling effusion, and pin fin cooling are additional methods of blade cooling. Since the different techniques have numerous advantages and disadvantages, the techniques use compressed air to cool the blades. The various cooling processes in turbine blade design can be found in Table 1 and the basic cooling designs are discussed below.

1. Internal cooling design: The convection cooling design uses cooling air that passes through the internal ducts of the blade, as shown in Figure 3a. Heat is extracted from the turbine blades via the convection process and the air moving through the blade also helps to decrease the blade temperature. To make this technique work effectively, the parts should contain large surface areas. The path of the air moving through the blade tends to be coiled spirally and complete with small fins. The shape of the passages inside the blade can be elliptical. Air travels from the hub through the tip of the blades to cool the blade design. However, the hot air outside the blade is relatively hot as it flows through the cooling channels and merges with the primary flow at the blade tip. Different convection cooling methods are available such as impinging design, which hits the inner surface with high-speed cooling air jets. Continuous air circulation improves the heat transfer rate compared to convection heating. The first set of blades in the turbine section experiences the highest load on the turbine. Therefore, the maximum temperature is observed at the leading edge of the blade and hence experience the thermal load. The central chords of the blades also use the technique of impact cooling (Figure 3b). The blades are hollow with internal cores and channels. The cooling air enters the leading edge and cools the fins that pass through the trailing edge [20].

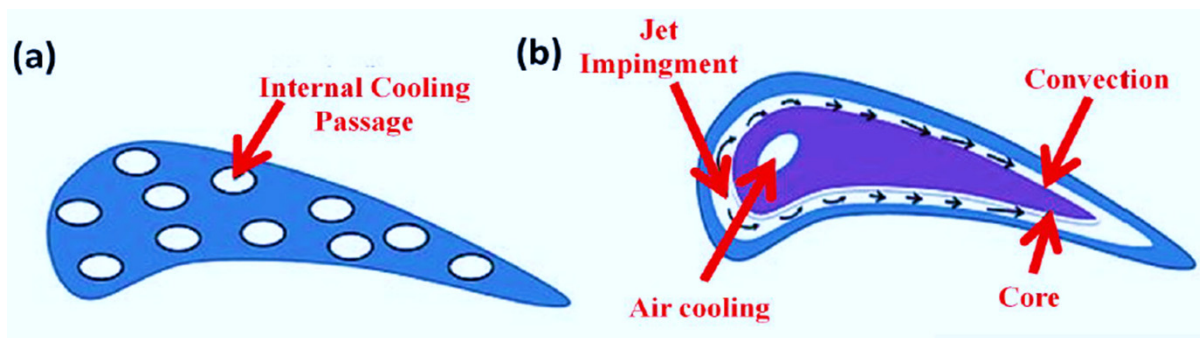


Figure 3. Blade cooling design by (a) the convection technique and (b) impact cooling [21].

2. External cooling: In addition to the cooling with techniques such as convection and impact, external cooling, also referred to as film cooling, is adapted. Air circulates through the small holes in the blade to decrease the temperature of the blade. The cooling air forms a thin layer on the outer surfaces of the blade. The heat energy transferred to the blade can exceed the melting point of the blade material of the blade whereas the heat extraction process improves the material ability and enhances the TET of the blade. Figure 4a shows the design of the film cooling turbine blade. The cooling efficiency is considered as the ability of the cooling system to extract heat from the blade surface. This efficiency depends on various parameters such as the flow of the coolant through the structure and the injection, velocity, momentum ratios, and density of the coolant. The injection geometry parameters have holes and slot geometry with injection angles. In the 1970s, the United States Air Force program funded several projects to develop the turbine blade for the military aircraft engine, which included both convection cooling and film cooling, which has become common for modern turbine blades [22]. Isentropic efficiency, air compression, and cooling systems increase the complexity of engine cooling. All of these factors contribute to the increase in overall engine performance as the TET continues to increase. Recently, researchers have recommended the application of a plasma actuator to cool the film [23]. In the design of effusion cooling, the surface of the blade is fabricated with materials consisting of porous structures that improve the surface temperature. The cooling air flows through the porous holes in the structure to generate a boundary layer on the blade surface. As the coolant circulates over the surface of the entire blade, uniform cooling is achieved. Figure 4b shows the design of the cooling of the blades by effusion. In the finned cooling design, the film-cooled trailing edge improves heat extraction of the entire blade. The design consists of pinholes and substructures to improve the cooling rate. Heat transfer occurs through the array of pin holes as well as the side walls. As the coolant flows through the fins at high speed, the separation of flows due to the fins produces wakes. Heat transfer depends on the type of fin pin used and the spacing between the fins. Transpiration cooling also generates a thin film of cooling air on the blade, which makes it similar to film cooling, but differs in that the air is 'leaked' using a porous shell rather than being injected through the holes. At higher temperatures, these cooling methods become effective because they form an even blanket of cool air on the blade. Transpiration-cooled blades are generally made with pores and strong structures. Therefore, the air must circulate through the various internal channels present in the structure before passing through the porous shells and finally cooling the turbine blade. The cooling of the film, the amount of air pushed through the blades, and the efficiency of the engine are related in such a way that the optimization is necessary to maximize the performance of the engine [20].

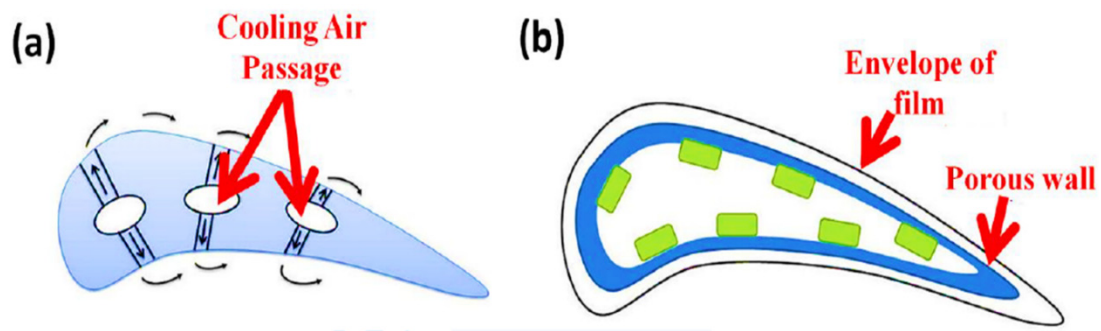


Figure 4. Design of (a) film cooling and (b) cooling by effusion [24].

Table 1. Evolution of turbine blade design.

Patent Number	Year of Publication	Patent Title	Description	Ref.
US3042371	1962	Variable camber balding	A variable camber in turbine blading is used	[25]
DE1903642A1	1970	Blading for rotors of axial compressor	Improvement in the blading system as well for the compressor	[26]
DE2144600A1	1973	Twisted and tapered blade for axial turbomachinery	Blade made in an aerodynamic fashion	[27]
US3837761A	1974	Guide vanes for supersonic turbine blades	Guide vanes are fastened to adjacent blades through a shroud ring, which has a converging-diverging opening	[28]
US3989406A	1976	Method of and apparatus for preventing leading edge shocks and shock related noise in transonic and supersonic rotor blades	Method for preventing leading shocks seen in blades operating at a transonic and supersonic condition and shock-related noise	[29]
US4131387A	1978	Curved blade turbomachinery noise reduction	A design to maximize the acoustic attenuation by the extension of upstream blades from the central hub	[30]
US4621979A	1986	Fan rotor blades of turbofan engines	The root section of a fan blade is contoured to an arcuate geometry	[31]
IL67806A	1986	Rotor assembly for gas turbine engine	Sealing the space present between the rotor blade and the engine casing	[32]
US4682935A	1987	Bowed turbine blade	Airfoil portion generates a compressive component of stress during bending due to centrifugal force	[33]
US4761116A	1988	Turbine blade with tip vent	Cooling fluids ducted into the interior cavities of blades to cool the blade during operation	[34]
US4826400A	1989	Curvilinear turbine airfoil	One design of an airfoil that consists of a pressure side and a suction side curved circumferentially outward in the direction that the suction side faces	[35]
US4808055A	1989	Turbine blade with restored tip	The worn tip of a turbine blade is restored by applying a metallurgically bonded wear-resistant surface at the tip	[36]

Table 1. Cont.

Patent Number	Year of Publication	Patent Title	Description	Ref.
US5017091A	1991	Free-standing blade for use in low pressure steam turbine	A design that avoids machining of a blade part by assembling in a row	[37]
WO1994012390A2	1994	Coolable rotor blade structure	The center of gravity of the airfoil sections is shifted forwardly in the outward direction to decrease tensile stresses in the trailing edge region	[38]
US5352092A	1994	Light weight steam turbine blade	The curvature area of the blade changes as the point of inflection is adjusted due to the presence of a high camber angle	[39]
US5503527A	1996	Turbine blade having tip slot	An airfoil with first and second sidewalls joined together at leading and trailing edges	[40]
AU684039B1	1997	Cooled blades for a gas turbine engine preventing or minimizing internal leakage	Sealing fluid is used to seal the gap between the turbine rotor blade tips and stator	[41]
EP0798447B1	1997	Turbomachine blade	Individual profile cuts are adapted to the radially variable flow angle and conditions. The shape of the airfoil is defined by threading the individual profile cuts	[42]
AU684037B1	1997	Cooled blades for a gas turbine engine	Convection cooling	[43]
JP2753382B2	1998	Axial flow turbine vane device and axial flow turbine	Improvement of a stationary blade of an axial flow turbine, and more particularly to an improvement of a stationary blade disposed of in an enlarged flow passage	[44]
EP0777818B1	1998	Gas turbine blade with cooled platform	Using compressed air to cool the platform with the blade root	[45]
US6071077A	2000	Swept fan blade	Blade consists of a leading-edge swept forward near the hub	[46]
US6312219B1	2001	Narrow waist vane	Stator vane includes pressure and suction sides extending cordially between the leading and trailing edges, and longitudinally between a root and a tip. The vane arrows in chord to a waist between the root and tip	[47]
US6168379B1	2001	Helicopter rotor blade with a movable flap	The actuator linkage comprises a fiber joint between the rod and the lever arm to transmit the actuating force to the flap or respective flap part. This feature makes it possible to actuate the upward and downward deflection of the flap using only tension forces	[48]

Table 1. Cont.

Patent Number	Year of Publication	Patent Title	Description	Ref.
US20030086788A1	2003	Three dimensional blade	Improved three-dimensional blade for an axial steam turbine comprising a leading edge with inlet flow angle and a trailing edge with an outflow angle, a pressure face, suction face, and a chord, which is the line connecting the leading and trailing edges	[49]
US6183202B1	2006	Stress relieved blade support	Relief grooves are provided to reduce the stiffness at the contact edges between the pressure faces to reduce peak stress	[50]
GB2409006B	2006	Tip sealing for a turbine rotor blade	Preventing or minimizing internal leakage of working-fluid (e.g., between stages for sealing space between rotor blade tips and stator using sealing fluid)	[51]
US6984109B2	2006	Rotor blade pitch control assembly	The trailing edge servo flap is located upon a trailing edge servo flap arm linked to the trailing edge flap. To pitch the rotor blade, the trailing edge servo flap is pitched in the direction opposite to the desired pitch direction of the trailing edge flap	[52]
CN100351495C	2007	Turbine blade pocket shroud	An improved gas turbine blade is disclosed that utilizes a blade tip shroud with tapered shroud pockets to remove excess weight from the shroud while not compromising shroud bending stresses	[53]
US20100215503A1	2010	Transonic blade	Provide a transonic blade that can reduce local stress at the hub cross-sectional surface while achieving a reduction in shock loss resulting from a shock wave on the tip cross-sectional surface	[54]
US7762770B2	2010	Hybrid actuator for helicopter rotor blade control flaps	Incorporation of the hybrid actuator for the main rotor blade control flaps	[55]
US7967571B2	2011	Advanced booster rotor blade	Sweep angle increases from the root as the first height location at the first-rate of change of sweep angle	[56]
US20110229321A1	2011	Vortex dynamics turbine	Active and/or passive control of the flow circulation around an airfoil as well as the momentum transfer to the flow close to the lifting surface to enhance its aerodynamic/hydrodynamic characteristics	[57]
US8414265B2	2013	Turbines and turbine blade winglets	Winglet is introduced	[58]
US8740567B2	2014	Reverse cavity blade for a gas turbine engine	Includes defining a cavity that extends from an airfoil tip section toward a root section of an airfoil section of a turbine blade	[59]

Table 1. Cont.

Patent Number	Year of Publication	Patent Title	Description	Ref.
US8894376B2	2014	Turbomachine blade with tip flare	Includes turbomachine system including a plurality of turbomachine blades coupled to a rotor, wherein each turbomachine blade has a blade base portion and a flared blade tip portion flared relative to the blade base portion.	[60]
EP2316988B1	2015	Wear-resistant and oxidation-resistant turbine blade	Use of abrasive and oxidation-resistant material on turbine blade	[61]
US9322282B2	2016	Fillet for use with a turbine rotor blade tip shroud	A fillet profile variable about the intersection as a function of aerodynamic air flow about the intersection	[62]
US9404368B2	2016	Blade cascade and turbomachine	A blade cascade for a turbomachine having a plurality of blades arranged next to one another in the peripheral direction, at least two blades having a variation to generate an asymmetric outflow in the rear area as well as a turbomachine with an asymmetric blade cascade, which is connected upstream from another blade cascade	[63]
CA2771349C	2017	Turbine blade with contoured platform	Flow path contouring is highly specific to two specific turbine stages and is not readily transferable to different stages whose efficiency and performance there could instead be degraded	[64]
US9995144B2	2018	Turbine blade centroid shifting method and system	Rotating turbine blade that tunes the natural frequencies of the blade is disclosed, which changes the second effective beam length of the blade, thereby changing the separation between the first natural frequency and the second natural frequency of the blade	[65]
US10443392B2	2019	Optimized aerodynamic profile for a turbine vane, in particular for a nozzle of the second stage of a turbine	Seven stage profile should enable the turbine to provide the desired efficiency; in order to increase the flow of air around the profile is sound over the working spectrum of the turbine	[66]
EP2725194B1	2020	Deutschland Ltd. & Co KG Turbine rotor blade of a gas turbine	The shape (tangent angle) of the circumferential or interrupted sealing edge is designed depending on the length of the profile so that flow separations are caused at the desired positions and flow separations are avoided at other positions	[67]

The arrangement of the ducts is an important parameter observed within the turbine blade. The blades in the Rolls-Royce Trent 500 turbojet engine, which have found their main application in the Airbus A340-500/600 commercial aircraft, feature a serpentine multi-pass design, as shown in Figure 5. Such revolutionary shift from single-pass convection cooling technology during the 1960s broke the barrier of consideration of the melting point of metal as a limiting parameter in the design of TET [68]. This serpentine cooling feature was

further developed in subsequent Trent engines. Airfoil cooling of these blades is provided by the multi-pass serpentine design and film cooling. As the TET of these engines exceeds 1500 °C, parallel cooling passages are present to cool the blade shroud. Additionally, the presence of complex 3D shaped film holes present on the leading and trailing edges increases cooling. The thermal capacity of the blades greatly improves when the materials are cast into a single crystal and coated with thermal barrier coatings (TBC) [10]. The unique design features observed in the turbine blade design were temperature margins, coolant supply, and blade tip design. First, the temperature margin characteristic refers to the relative reduction in the coolant inlet temperature when the pre-turbulence nozzles orient the direction of the cooling air in the rotational path of the blade. This causes air to expand in the channels as it absorbs heat to decrease the temperature in the blade before exiting the cooling passage with high velocity. Second, some prefer coolant while Rolls-Royce prefers to use the air present on the high pressure (HP) and low pressure (LP) side to cool the blade. The leading edge, which supports most of the load during service, is cooled using HP air that circulates in the main cooling circuit by providing film cooling. The LP air is responsible for cooling the leading edge with convection cooling. With one major drawback of the thermal stresses produced by the temperature difference of the HP and LP gases, engineers must optimize the trade-off between performance and drawbacks. Finally, the blade tip design is also an important criterion, as turbine performance weakens with over tip leakage (OTL) and leak vortex. These leaks occur due to the gap between the tip of the rotating blade and the turbine housing and the pressure difference on both sides of the blade caused by the gap. Rolls-Royce has also patented a tip sealing method for unshielded turbine blades, which is often used in military engines to minimize tip leakage. It features a gutter on the tip of the blade that during operation will trap the leak flow in the gutter. As a result, a vortex is created that guides the airflow through the gutter to the trailing edge toward an exhaust. This allows for leakage from the tip and avoids the leakage flow in the mainstream [69].

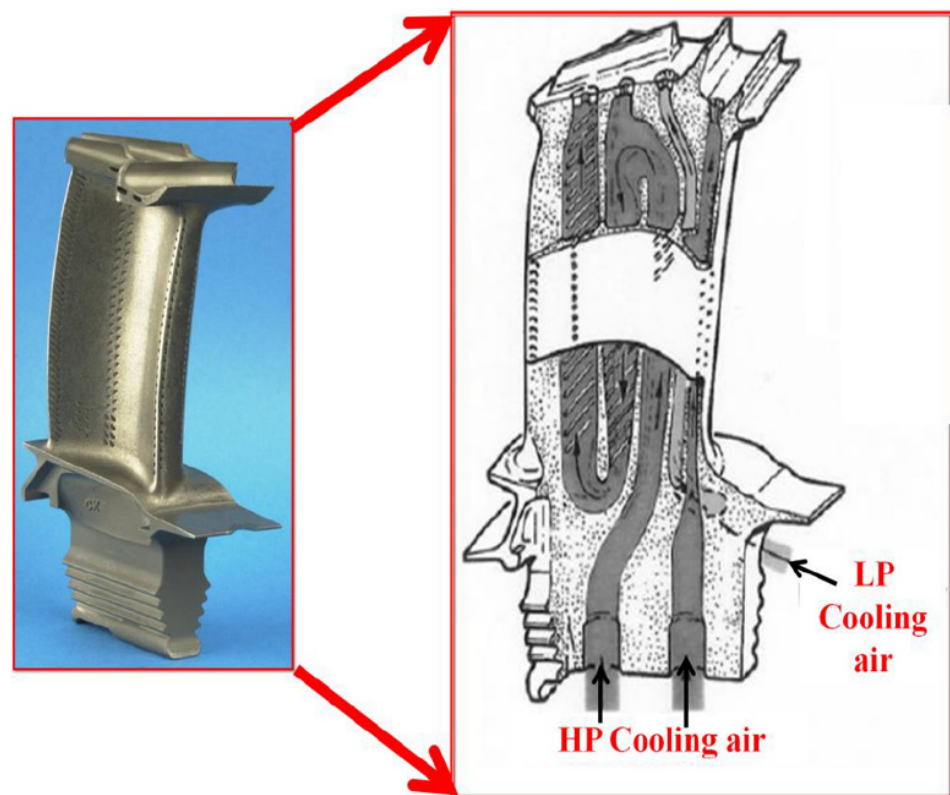


Figure 5. Trent 500 HP turbine blade [70].

Gradually, thermo-mechanical simulations of generalized honeycomb materials were used to derive the design that was applied to local properties to reduce the development of stress during operation [71]. Consequently, a significant lowering of maximum temperature and stress during the operation was reported. Furthermore, uniform stress and temperature profile were observed due to the replacement of hollow air channels with porous structures that also help to support the structural load, better heat conduction throughout the blade, and greater surface area for the transfer of heat. In addition, design optimization to reduce the weight of any component can improve operational efficiency. However, the architectural materials of turbine blades currently face three limitations. First, the study reports that homogenized stress within the honeycomb and locally present stress concentrations are neglected. It was also observed that some significant stress states were present. Second, the smooth transition from one domain to another is not taken into account. Finally, the simulations take into consideration only the static loads and their responses [72]. The findings in the study generate interest and encourage further design studies. It fits perfectly into the area where the most actively sought rails to improve turbine engine efficiency. For military aero engines, a unique tip sealing configuration is patented by Rolls-Royce for turbine blades, differs from the orthodox flat tip or the creaking tip, and is applied to the EJ200 HPT blade design as the technique reduces air leaks from the tips. As described in the patent, a gutter is present in the tip of the blade that is wider than the blade in comparison to the trailing edge of the blade, and a section of the gutter diverts the air toward the lateral pressure. In the application, the gutter traps the escaping gas. This creates a vortex and allows air to pass through the gutter channel and exit through the trailing edge [73]. There is a need for an optimized blade design to increase the efficiency of cooling and loading during the service of the turbine blade. In this regard, a different approach from the conventional techniques is essential. Various manufactures have explored AM and have observed good results. With the increasing flexibility of parts produced by AM, the manufacturer has focused on producing light and creative parts. This approach aims to generate parts with the same performance as conventionally manufactured materials by reducing the weight and material waste without compromising the structural integrity of the material. One way to achieve this is to optimize the surface topology. In the case of turbine blades in gas turbine engines, the possibility of changing the shape is low. Therefore, the cavity in the blades is optimized in several strategies to improve the efficiency of the cooling and loading methods in the leading edge. In internal lattice models, the upper shape of the airfoil remains the same as the component becomes lighter than in the conventional design. Using simulation packages, lattice structures are simulated for different parameters to find the optimized output based on the applied loads in service in a static simulation. Porous materials are designed rather than porous structures. Metallic lattice is a popular porous structure. Therefore, when dealing with porous materials, it is essential to predict the shape, size, position, and orientation of the elements present in the cells. The beam-based lattice structure is a popular option in cellular structures. However, generative designs are alternative ways of researching porous structures inspired by nature. An invention by Hinckley and co-workers, attributed to Raytheon Tech corp., presents a turbine blade design in which the blade cavity is occupied by a lattice network [74]. The cavity is defined as the hollow region occupied between two edges and two side walls. The cavity is filled with a lattice network that connects the two side walls. The airfoil includes a cavity, a lattice network, and a damping element that floats along with the lattice network. These observations conclude that the lattice structure of the turbine blades exhibits the ability to improve the life of the turbine blades through efficient cooling of the blades. Various patents for the additive manufactured blade design that have been implemented in the aviation industry are given in Table 2.

Table 2. Patents based on additive manufacturing in turbine blades.

Patent Number	Year	Patent Title	Design Pattern	Ref.
JP4223637B2	2001	3D free shaping method and 3D free shaping apparatus	A three-dimensional model made of an intermetallic compound by the stereolithography technique	[75]
EP3179042B1	2017	Gas turbine engine component having engineered vascular structure	The step of forming the vascular engineered lattice structure includes forming a core using an additive manufacturing process and using the core to cast the vascular engineered lattice structure	[76]
US20160339516A1	2017	Method for forming components using additive manufacturing and re-melt	The component is a rotor blade made up of single crystal metal	[77]
US20190063229A1	2019	Turbine blade having an additive manufacturing trailing edge	An additive trailing edge is disposed on the trailing edge of the airfoil, wherein a first material of the trailing edge of the airfoil is different from a second material of the additive trailing edge, and wherein a first radius of the trailing edge is larger than a second radius of the additive trailing edge	[78]
EP2896786B1	2019	Turbine rotor assemblies with improved slot cavities	In a third step 1730 aircraft, the turbine rotor blade is formed. Any suitable manufacturing technique may be provided including casting and additive manufacturing techniques	[79]
US20160369634A1	2019	Airfoil and method for manufacturing the same	The method includes three steps: (1) forming the first section using a casting technique; (2) forming the functionally graded section on the first section using an additive manufacturing technique; and (3) forming the second section on the functionally graded section using an additive manufacturing technique	[80]
US10525525B2	2020	Additively manufactured core	The method includes integrally building at least one trunk and the skin core with the additive manufacturing system	[81]

4. AM Techniques for the Fabrication of Turbine Blades

A turbine blade requires printing of high-temperature materials that are super-alloy constituents. Various AM techniques that are implemented to build the turbine blade are discussed below.

4.1. Selective Laser Sintering (SLS) as an Initial Powder Bed Fusion Process

During the 1980s, with the support of DARPA, Dr Deckard and Dr Beaman of the University of Texas at Austin developed and patented the additive manufacturing technique of selective laser sintering (SLS). As the SLS patent expired in 2014, the technology has been open to research. Sintering in SLS fabricates the 3D structure from the fused state layer with micro-sintering. Necking is a phenomenon observed during sintering that occurs due to the reduction in viscosity. The surface coating that acts as a binder is melted with the help of a laser. Here, the materials attempt to reach the minimum free energy state, which results in a diffusion that takes into account the movement of molecules between particles, becoming a major driving force in this process. SLS uses a laser (for example, a carbon dioxide laser) to join small particles of various material powders into one piece with a designed three-dimensional shape. However, the SLS process uses lower laser power, typically used for polymers and nylons in recent days. An advanced version of this process with high laser powers is used in the case of metals, which is discussed in the next section.

The laser selectively sinters the powder material while scanning the cross-sections onto the powder spread by the CAD file. Since the density of the final part is subject to process parameters such as the maximum laser power, instead of the laser duration, pulsed lasers are typically used in the SLS process. A Gaussian distribution is observed in the size distribution of the powder particles, although the process can be adapted to suit the thicknesses of the layers in the process. Figure 6 shows the SLS manufactured fixture and an unassembled single turbine engine. However, these parts have porous surfaces; these can be treated using various post-processing techniques such as metallization, oven enameling, vibrating grinding, tank coloring, gluing, powdering, coating, and flocking [82].

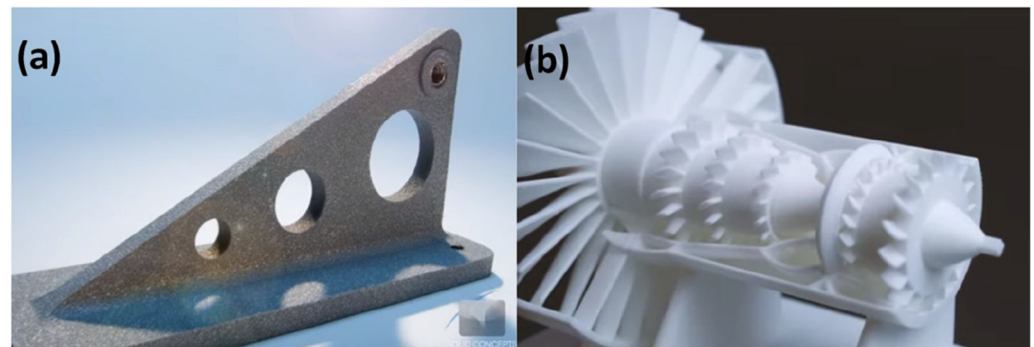


Figure 6. SLS manufactured (a) fixture and (b) single part turbine.

4.2. Selective Laser Melting (SLM)/Direct Metal Laser Sintering (DMLS) as Currently Used for Metals

Selective laser melting (SLM) is a powder bed process that uses a high-intensity laser to melt the powder in a layer. The structure is generated from a CAD file that is sliced into thin cross-sections or layers. These data are converted to an STL file readable by the printing machine that supports any complex design. The build process begins with a thin layer of metal powder spread on the substrate plate in a build chamber. The high-energy laser scans the cross-section to fuse the powder into the regions described in the STL file. When the scanning is complete, the build platform lowers and another layer of powder is spread over the substrate and the process is repeated until all the layers are scanned and built one on another to create the 3D physical model. During the process, high temperature is required for melting, the production chambers maintain an inert or vacuum atmosphere to control the oxygen content to avoid oxidation and other problems affecting the properties of the produced turbine blade. Laser power, hatch distance, layer thickness, scan strategy, and scan speed are the parameters primarily used to optimize the process. When heating and fusing occur, the heating capacity depends on the mass and materials. When the energy is insufficient due to the mixing of low laser power, large layer thickness, and high scanning speed, it generates a balling phenomenon due to insufficient surface wetting. This deteriorates the quality of the product. Additionally, increasing the hatching distances results in regular porosity because the powder does not fuse well together. To achieve complete densification of the part, optimized minimum energy is required. A certain degree of overlap also ensures sufficient densification. SLM operating parameters are modified to improve surface quality. Figure 7 shows the steps involved in the SLM process to build the products. The final parts require post-processing techniques such as sand blasting, machining, and electro-machining. The tensile properties of SLM parts can be superior compared to traditionally manufactured parts. Compared to casting, SLM reduces building time, which is of high value in aero-structures [83]. Not only printing the products, SLM also offers the ability to assist in the repair and maintenance of the worn and burn-out parts faster and easier than the traditional repair methods. An example of this is the repair of the worn-out burner tip exposed to hot gas in the combustion chamber developed by Siemens in 2013. Siemens has developed a customized SLM machine that can repair the parts quickly and also economically. Such a method of SLM-based repair leads to a much

smaller area of the burner tip being removed and replaced. As a result, the repair time is reduced to 90% of the usual time.

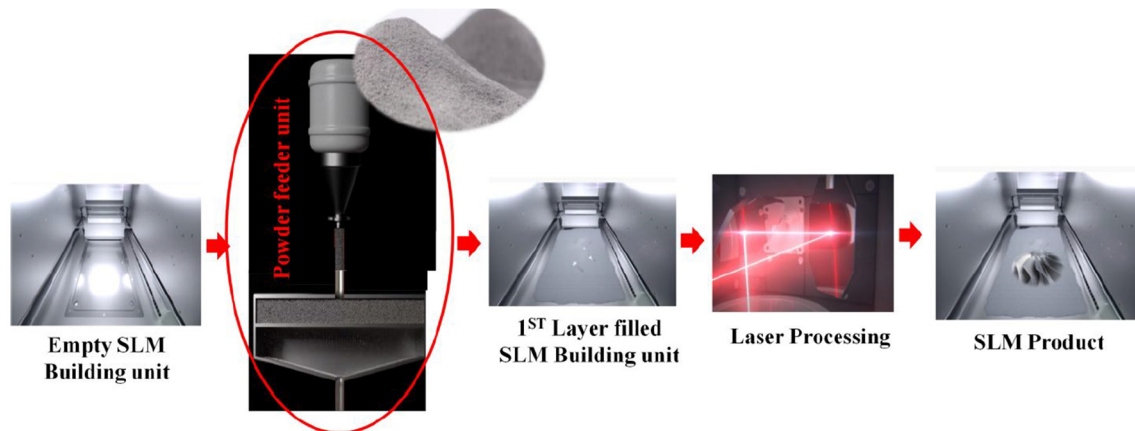


Figure 7. SLM process sequence in the building unit.

Recently, Siemens designed newer turbine blades to be manufactured using DMLS technology [3,84]. In collaboration with Material Solutions, the turbine blades were successfully 3D printed on an Eosint DMLS machine using a nickel super-alloy powder. The 3D printed blades were tested on a 13-megawatt SGT-400-type industrial gas turbine under full-load conditions. The blades were found to withstand extreme pressures and temperatures of about 1250 °C at 13,000 rpm. With the adoption of AM, the design and development of the blade went from component design to testing in just 18 months, which otherwise would have consumed six months. These blades had improved internal cooling geometry, which was possible because of the design flexibility of AM. The 3D printed turbine blade made up of a Ni-based super alloy developed by Siemens is shown in Figure 8.



Figure 8. 3D printed Ni alloy based turbine blade by Siemens [85].

4.3. Electron Beam Melting

Electron beam melting (EBM) is an additive manufacturing process that uses an electron beam to melt and fuse the metal powders spread on the platform in a controlled

atmosphere. The energy density in the electron beams is controlled by electromagnetic coils to increase the melting capacity, thus leading to an increase in productivity compared to SLM machines. Absorption of the electron into the material generates a negative charge, which can generate a repulsive force around the powder particles that can throw the finer particles from the powder bed, creating a powder cloud. In addition, the increased negative charge can also reflect the incoming electrons, creating more beams for diffusion. Consequently, the powder bed must be conductive to be processed with this method. Adjacent scanning strategies must also reduce the formation of these negatively charged particles in a particular location. As a result, the size of the melt pool increases, which decreases the resolution of the parts produced. In the aerospace industries, EBM is used to produce the quasi-shaped component and electric discharge machining (EDM) is applied to obtain the final shape [86]. EBM is associated with a greater thickness for each layer of powder; while increasing production rate creates an inferior surface finish, the powder remains in the 45 μm to 150 μm ranges. However, using smaller particles can produce a higher surface finish while productivity suffers. Therefore, the EBM process results in lower resolution and higher surface roughness than SLM. The remaining loose powder can be recycled in EBM, which contributes to effective use of the material. One of the advantages of EBM over SLM is that EBM parts are always produced in a vacuum chamber, resulting in less absorption of impurities throughout the entire process. Fewer impurity uptake facilitates the production of highly reactive materials. Residual thermal stresses are a major concern due to the increase in the cooling rate and the temperature gradient. This involves heating the powder bed to reduce the temperature gradient. In the case of EBM, minimal residual stress is observed compared to the SLM manufactured parts. However, preheating the powder bed can increase powder size by sintering. In this case, the size of the powder is reduced by prior grinding, which is a part of EBM processing, to maintain the optimum particle size [87]. Figure 9 shows a turbine blade fabricated using the EBM technique.



Figure 9. Turbine blade fabricated using the EBM technique [88].

Recently, Avio Aero, a General Electric (GE) Aviation company, has installed 35 AR-CAM EBM machines in the USA and Europe, which will be primarily focused on printing TiAl turbine blades on the LPT of the latest massive GE9X engine [9]. The GE9X engine

was developed for Boeing's 777X Jet engine, the world's largest jet engine. These Arcam EBM machines use a powerful 3-kilowatt electron beam to melt the final grains of TiAl powders to build 40 cm long blades. The TiAl is a high melting point alloy and is also a strong material. GE has observed that the additively manufactured TiAl blades weighed 50% less compared to the traditional Ni-based alloy blades. Such weight reductions are expected to reduce the fuel consumption by 10% as well as the emissions compared to its GE90 engine. Such contributions are significant achievements in the aerospace industry. At their facility, GE can print six TiAl blades per batch using Arcam EBM machines. The additively manufactured TiAl blades spin at 2500 rpm inside the engine and withstand searing heat with a huge amount of force. The 3D printed GE that made TiAl LPT blades is shown in Figure 10.



Figure 10. The 3D-printed TiAl blades for LPT of the GE90X engine [89].

4.4. Binder Jetting Process

The binder jetting process is another family of additive manufacturing processes in which the selected binder is deposited onto the powder bed selectively. The binder creates bonds between the particles to form a solid part in a layer. Using this process, granules of metals, sand, and ceramics are processed to form solid parts [90–92]. Since the raw materials are not processed directly to form the solid product, but rather the binder only binds the powder particles, leading to low sinterability of the particles. Hence, the density of the products is not up to the mark, especially in the case of ceramic powder based products, and thus the properties of the products are not adequate. Several attempts have been made to improve the density of the product, which depends on the powder particle size that relates to the flowability, choice of binder, building parameters, equipment specifications and parameters, and design of the product to be built, etc. [93]. Recently, Air Force Research Laboratory (AFRL) in the USA has collaborated with Exone, a binder jetting 3D printer manufacturer. The contract was given to qualify AF-9628, a high-strength steel produced by the U.S. Air Force, for binder jetting. Although AF-9628 parts were produced by other additive manufacturing techniques such as PBF, the binder jet process was found

to print the parts more economically. Interestingly, these binder jet printed parts were 20% stronger than those processed by other AM techniques [94].

4.5. Laser Cladding

The principle of laser cladding is to use a metal filler in a very thin layer to fuse different layers and ensure a metallurgical bond between the different substrate surfaces. The laser beam can distribute a precise and localized heat input to the fillers. In industrial applications, laser cladding is used for rapid manufacturing, part repair, surface coating, and the development of innovative alloys. In particular, laser cladding is a flexible process that can fabricate functionally graded materials and heterogeneous components due to its ability to mix more than one type of powder by controlling the feed rate of each process. In addition, the technology enables the design at a microstructural level by varying the gradient of the material with localized fusion and the strong mixing motion present in the melt pool. Thus, the materials can be structured for flexible functional performance in their respective applications. The complex thermal history associated with the rapid heating and cooling rates of the technique allows for prolonged solid solubility in metastable phases or the production of non-equilibrium phases. CLAD requires accuracy as the part is produced by finer deposits, an optimized setting, and exact geometric control over the features of the deposits. The CLAD nozzle ensures that the input of metal powder melts them to generate the maximum yield of multidirectional deposits while ensuring optimal gas coverage [95]. Figure 11 shows the morphology of the laser coating of Stellite Grade 6 on carbon steel [96].

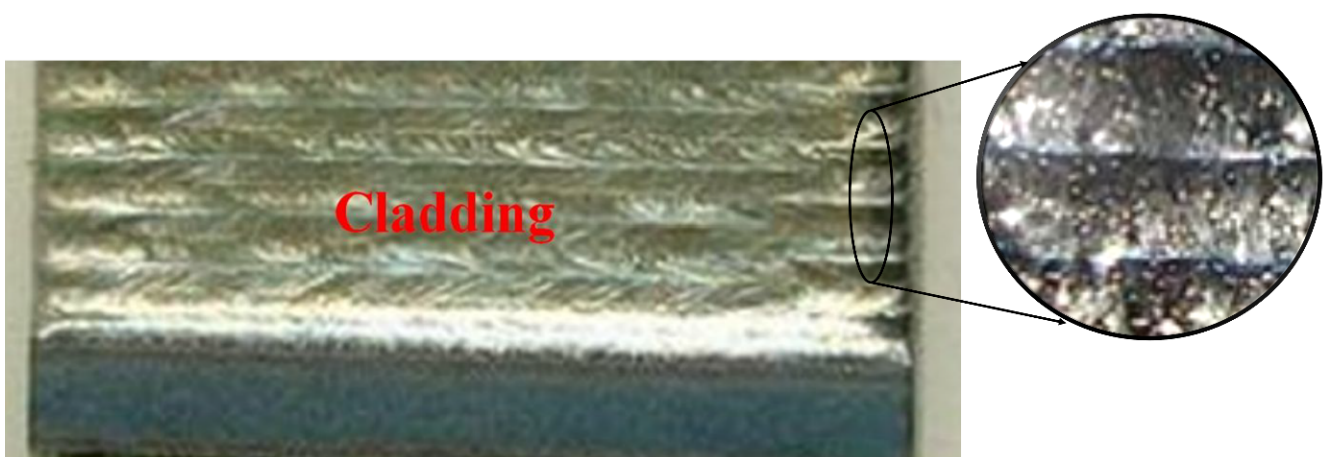


Figure 11. Side view of the morphology of laser cladding in grade 6 Stellite on carbon steel [97].

4.6. Laser Engineering Net Shape

Laser powder forming, also known as proprietary (Laser Engineering Net Shaping, LENS), is a sub-category of direct energy deposition (DED) process, focused on manufacturing metal components directly from the CAD file using a metal powder injector directed to the molten pool. The molten pool is made using the laser heat source. The process can produce structures with near-net-shape parts with complex geometries where, conventionally, it is difficult to manufacture parts with exact specifications. The greatest advantage of LENS over SLS, SLM, and EBM is the size of the product that can be printed. The build volume in LENS can go up to several feet, while it is a maximum of 40 cm in the latter cases. A laser melts the injected metal powder at the focal point of its heating source with a deposition head. The laser beam usually travels through the center of the head. The laser is further focused using lenses [98]. The X–Y table moves with patterns defined to produce the different layers of the part. A new layer of powder is sprinkled on the last layer and the platform is lowered. Gravity or pressurized carrier gas are suitable means for dispensing and distributing metal powders around the circumference. Layer-to-layer adhesion improves from a higher wetting surface. Shielding gases protect the weld pool from oxidation

and other atmospheric impurities during production. Selective laser sintering is similar to LENS in many ways and contrasts metallic powder as a powder applied directly to the deposition location at that moment. A wide range of alloys including titanium, stainless steel, aluminum, and other special materials can be made from composite materials and functionally graded materials [99]. In addition, Optomec's laser cladding technology and LENS metal AM systems that are based on a directed energy deposition (DED) process are also used in turbine blade applications to repair turbine blade tips. Figure 12 shows the repair of a turbine blade using an Optomec made AM machine system [100].

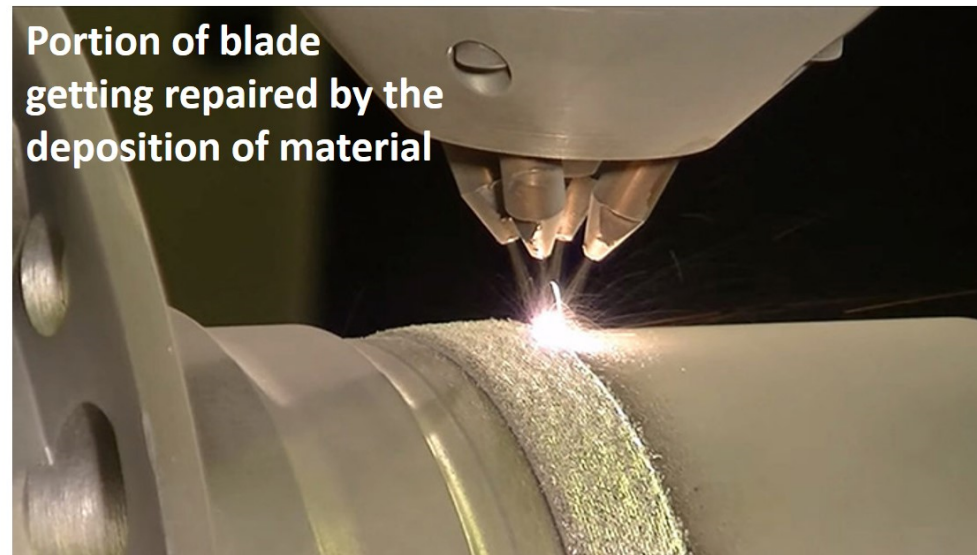


Figure 12. The Optomec DED technology to repair a turbine blade [101].

4.7. Electron Beam Free-Form Fabrication

Electron beam free-form fabrication (EBF3) is another process of the DED family, a method that fabricates parts, which are close to near-net-shape (Figure 13). This saves raw materials, which offers a great advantage over traditional practices. On a metal substrate, a focused electron beam creates a molten pool in a vacuum environment that helps to generate a cross-section. The practice of electron beam welding for additive manufacturing was first founded by Vivek Davé in 1995 in his doctoral thesis at MIT. However, EBF3 was a name given by the NASA team that developed the process. Karen Taminger, materials research engineer for NASA's LaRC, was primarily responsible for developing the use of electron beams in additive manufacturing to further improve the manufacturing process. Therefore, EBF3 is a NASA patented additive manufacturing technique used to fabricate near-net-shape parts with less material and workmanship. EBF3 is a method that can build metal parts in zero gravity environments. This additive process uses a solid feed stock that is melted using an electron beam to produce metal structures [102]. The advantages and capability of the process make it interesting to fabricate parts in space. Currently, the titanium spars for the vertical tails of the F-35 Joint Strike Fighter are manufactured using this manufacturing technique. Reduced titanium waste and shorter processing times have led to an increase in production rate and resource savings for the company, Lockheed Martin, and Ferra Engineering, based in Brisbane, Australia, intend to open the first factory in the world for the production of the F-35 components. EBF3's ability to control the performance of its aircraft components by controlling material properties has drawn a lot of attention to this process. The EBF3 method is scalable for various applications as it can accommodate sizes ranging from inches to a few feet depending on the size of the chamber [103].

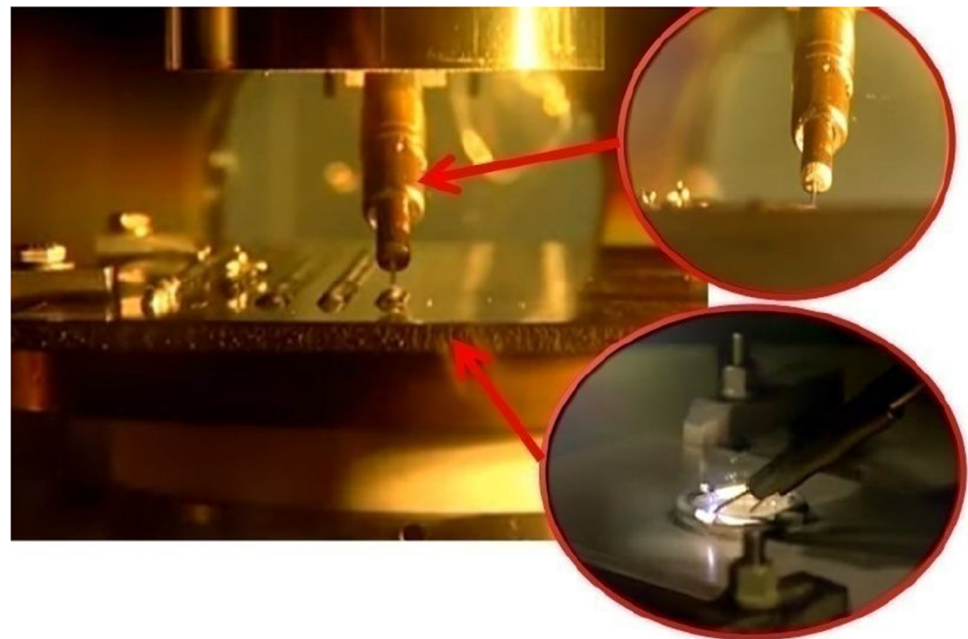


Figure 13. Electron beam freeform fabrication technique showing the first layer building in the layer-by-layer process [104].

4.8. Aerosol Jet Process

The aerosol jet process is a patented technique of electronic and metal 3D printer manufacturer, Optomec, which is based in New Mexico. It is a trademark of Optomec, which is a company that has been developing AM solutions since 1997. The company offers an exciting area of 3D printing that includes the printing of sensors. Such sensors that are part of advanced control and monitoring systems can be printed on the turbine blades. This increases the efficiency of monitoring the turbine blades during operation. Figure 14 shows the 3D printed turbine blade that is integrated with creep sensors to monitor the structural health of turbine blades [105]. Such advanced design features can be brought into reality only by additive manufacturing.

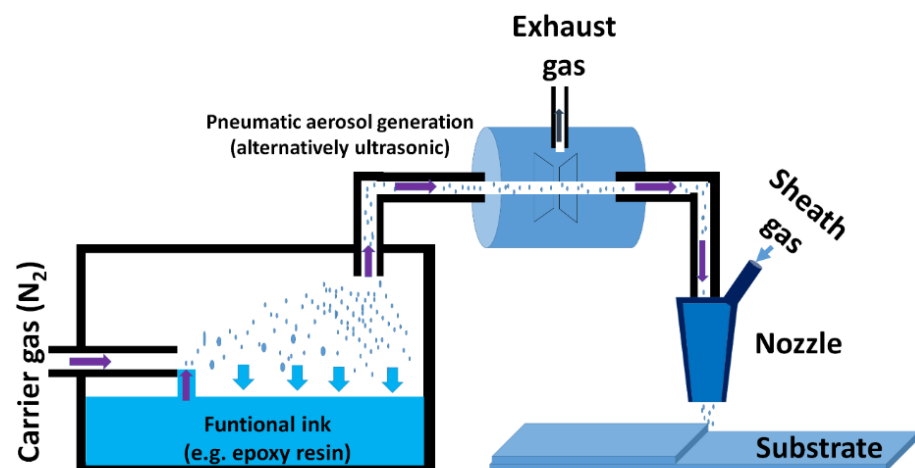


Figure 14. Aerosol jet process [106].

Optomec Company offers an exciting area of 3D printing that includes the printing of sensors. Such sensors that are part of advanced control and monitoring systems can be printed on the turbine blades. This increases the efficiency of monitoring the turbine blades during operation. Figure 15 shows the 3D printed turbine blade that is integrated with

creep sensors for monitoring the structural health of turbine blades [105]. Such advanced design features can be brought into reality only by additive manufacturing.

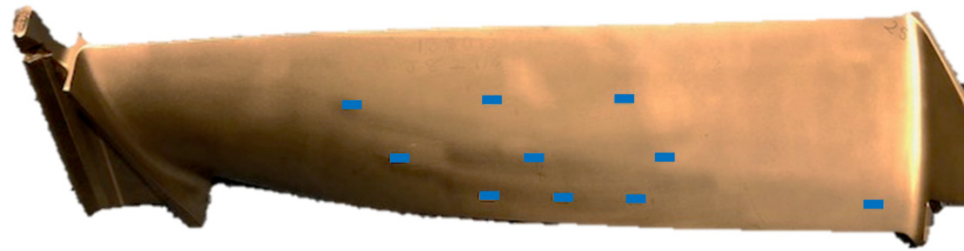


Figure 15. 3D printed sensors integrated turbine blade [105].

5. Processing Parameters

On the basis of various working principles, several parameters affect the processing of turbine blades. The effect of all those parameters is observed in the build quality of the turbine blade. Optimized process parameters of each process plays a great role to print a good quality blade. Hence, a better understanding of the influencing parameters for a chosen technique is highly essential. In general, with such a high melting point, super alloys can be processed using several AM techniques, as discussed in the previous section. In particular, we discuss different influencing parameters in the SLM process for the turbine blade fabrication in comparison to all other AM techniques.

5.1. Particle Size and Shape of Powder That to Be Printed

Turbine blades operate in extreme conditions and hence the blades are made up of exotic super alloys that can withstand extreme conditions. In these kinds of processes, the starting material is generally in the form of powder. Hence, an understanding of the powder particle size and distribution is essential. During processing, the powder of different particles' shapes and sizes are blended to achieve the packing density of the powder bed, avoiding the separation or segregation of particles in the bed. The powder bed fusion processes are carried out by spreading a layer of powder and then scanning the layer using a laser heat source to create a solid layer [107]. Therefore, the characteristics of the powder bed play an essential role in influencing the final properties of the final part produced. A layer of powder spread on the building platform corresponds to the thickness of the layer of the part that is sliced in the 3D model. This in turn affects the porosity and density of each layer. Particle shape as well as the distribution of the particle size and shape affect the layer thickness. Depending on the method used to produce the powder for the process, the powder can be varied from spherical to extremely irregular. In general, the powder is processed by gas atomization techniques to obtain fine granules of super alloys such as NiTi, TiAl, etc., and the particles are usually spherical. Particle size varies with the type of processing technique chosen that corresponds to the thickness of the layer. The powder must consist of spherical particles of the same size or with a narrow particle size distribution. The density of the powder in the layer influences the heat transfer characteristics of the bed along with the material flow due to heating [108]. In addition, the strong dependency of the particle packing in the bed is associated with the thermal characteristics during the manufacturing process [109]. Inter-particle pores are found by spreading the spherical powder in the layer. The fractional solid volume of each particle X_i considered in the bed of PBF can be measured as its solid volume divided by the total solid volume of all particles, as shown in Equation (1).

$$X_i = \frac{S_i}{\sum_{i=1}^n S_i} \quad (1)$$

where S_i is the solid volume of spherical particles. Gas porosity and other defects can be reduced by improving the particle packing and heat transfer characteristics of the

powder bed to maintain uniform heat distribution. On the other hand, the packing of non-spherical particles will prevent the part from maximizing its dense configuration. Both ellipsoid and spheroid shapes exhibit packing behavior typically attributed to non-spherical particles. The consistency in the particle shape can result in blades of maximum density. Any deviation from the ideal shape can lead to the formation of disordered packing with a structure similar to a random spherical packing, and thus the density decreases. Similarly, as the height/width ratio of the powder bed increases, the density decreases. The transition from spheroidal to non-spheroidal shape can be made by adopting prior particle reduction processes such as cutting, elongating, or deformation processes. It is often found in experiments that lower densities are the result of the packing of smaller particles [110]. Additionally, after the threshold limit of the particle size, the effect of gravity is no longer the dominating factor, and inter-particle forces such as van der Waals forces and electrostatic forces become increasingly relevant. At approximately 100 μm in particle diameter, the ratio of inter-particle force to particle weight is greater than unity. This results in the creation of agglomerates due to the influence of a strong cohesive force. On a macroscopic level, particles behave individually. The morphology of the particles significantly influences the bulk packing as well as the flow characteristics of a particle. Consequently, highly spherical particles are generally more favorable in the AM process. There is also an increase in the flowability of the powder, which has a narrower particle size distribution and contributes to better strength and hardness of the blades. Investigations into the application of various particle size distribution have shown that the distribution also significantly influences the quality of the printed part and control over the particle size distribution tends to control the surface roughness of the final product [111].

5.2. Powder Bed Density

It is quite evident from the previous section that the particle size distribution significantly affects the final powder bed density and hence the mechanical properties of the blade. A large variation in the density of the powder can lead to the production of rough and porous blades with poor mechanical properties. In addition, the calculation and determination of density such as the tapped density and the apparent density cannot be an accurate reflection of the actual density of the formed powder layer or bed. Therefore, the density of the powder bed is an essential parameter to be understood and studied to estimate and control the shrinkage in the final part PBF structure [112]. Furthermore, the density of the powder bed is associated with the green density. Particularly during densification, less shrinkage can be ensured in powder beds with higher green density. One of the main obstacles in the process is to adjust the porosity of the powder bed so that the final part is made up of a uniform and maximum density. In this case, the density of the powder bed affects the heat transfer rate from the laser, making the thermal conductivity and absorption of the source power that are important considerations for improving and maximizing the density of the produced part. Many standards assess the packing of the powder bed, which depends on the density or manufacturing technique used [113]. The random packing density increases exponentially as the particle shape deviates from the perfect sphere as per Equation (2). The cumulative weight fraction (W) can be calculated as,

$$W = A \times D^q \quad (2)$$

where D is the particle diameter and A and q are empirical constants. The best results of the bulk density were obtained for values of q between 0.5 and 0.67. Additionally, through the application of powders with a larger particle size distribution, a similar effect on bulk density was observed. In this case, a higher density was observed because the smaller particles occupy the void space of the structure [114]. True density is characterized as an inherent property of a material and the apparent density that accounts for the voids. The determination of the tapped density and apparent density does not essentially reflect the density of the powder layer or the powder bed. Apparent density reflects the condition of loosely packed powder and is determined using ASTM B212. The various terms used

for powder density are powder bed density, bulk density, or packing density [115]. Bulk density is mainly influenced by the distribution of the shapes and sizes of the particles. Bulk density is critical in determining certain material specifications and obtaining guarantees on the structure of the powder bed and the flowability of the powder. It is necessary to characterize the final product and also to measure the volume of intricate and complex finished products [116]. Devices by Micromeritics Instrument Corp. such as the AccuPyc™ II 1340 gas displacement pycnometry system [117], GeoPyc Envelope, and Density Analyzer [118] can be used to determine important parameters essential to standardize AM process parameters. It also acts as a possible indicator for evaluating the properties of the final product. Integrating the true density from an AccuPyc measurement means porosity can be established quickly and easily. Both of these tools use non-destructive testing methods and can be used to determine the final porosity of products [119]. However, many factors cause the variation in AM product density results even when external factors are ruled out as constants during the process. The factors with the greatest effect are the laser/beam power parameters, the processing environment (i.e., humidity, presence of inert gas), or the properties of the metal powder (particle size, particle shape, distribution, or flowability) [120]. The best morphology can be observed in powders made with the gas atomization technique. A moderately lower packing density tends to improve the convection of fluids aspirated with the aid of gravity. The downward flow of fluids tends to increase the hydrodynamic instabilities of the melt, which leads to the generation of defects such as “balling” defects. Balling occurs due to the breaking and discontinuities in the molten pool produced during the SLM, increasing the probability of mechanical defects and surface defects. As the average packing density increases from 38% to 45%, the discontinuous weld pool is eliminated to create a smoother surface [121].

5.3. Residual Stresses

Due to the laser heat source, a local thermal gradient is introduced with a local phase or volume change during processing of the blades. Consequently, residual stress is a major problem in many AM techniques. Residual stresses are self-calibrated and persist even after their manufacture. Residual stresses also exist without thermal gradient and additional external forces. Generally, stresses develop from misfits in different regions and the different phases within the blade. Understanding residual stress is critical because it leads to several undesirable consequences on material properties such as poor fatigue resistance and critical failure during operation [122]. Residual stress can be estimated using methods such as the hole drilling method, the deflection method, the X-ray diffraction method, the contour method, and the neutron diffraction. Several computer simulations have been established that use the finite element method (FEM) to understand residual stress development related process parameters in AM, the melt pool, and resulting gradient on a microscopic scale. On a macroscopic scale, studies have been performed to estimate deformation and macro-stress in the parts produced [123]. In many cases, the numerical simulations assist in understanding the residual stresses distribution while accounting for laser parameters and scanning strategies. The history of the transient temperature present during the solidification is crucial to estimate the final residual stress in the built part and the distribution of thermal stresses. These stresses can cause part failure by distortions, delamination, or cracking [124]. Energy dispersive diffraction can be used to investigate the structure and residual stress gradients near the surface region. In diffraction, the relationship between a lattice spacing d_{hkl} and the corresponding diffraction line E_{hkl} is easily derived from Bragg's equation. Furthermore, depending on the absorption of the material as well as the scattering angle, the residual stresses are estimated using Equation (3) [125,126].

$$d_{hkl}(\text{\AA}) = \frac{6.199}{\sin \theta} \left(\frac{1}{E_{hkl}(\text{keV})} \right) \quad (3)$$

In the case of additive manufactured Ni-based super-alloys, it is difficult to lower the residual stresses. Generally, these residual stresses are eliminated and managed with

the help of heat treatment. It is important to reduce the thermal stresses induced in the 3D-printed metal parts. There is scope for improvement in platforms that use physics-inspired scanning strategies that aim to reduce thermal stress by adjusting temperature gradients in complex 3D parts. Simultaneously, hot powder bed systems used in electron beam-based platforms should be extended to laser systems to relieve residual in situ stresses, for example, selective electron beam melting systems [127]. Heating the end-use part to a temperature above 570 °C would eliminate any residual stress and even residual compressive stress, which would improve the fatigue performance of the turbine blade. Thermal gradients present near the substrate leads to inhomogeneous microstructures [128]. Regulating the scanning strategy can also be an effective tool to reduce residual stress. Concept Laser has developed a creative Laser CUSING® approach in which the scanning strategy is selectively adjusted using an algorithm to minimize the expected residual stresses. In addition, applying a compressive mechanical load with laser shock peening (LSP) or rolling on the surface of the fabricated part to cancel or decrease the amount of residual tensile stress is another approach to in situ control of residual stresses in AMed metal. Some of the literature [129] discovered the ability of LSP to regulate residual stresses in SLM and found that residual surface tensile stress could easily be transformed into beneficial residual compressive stress with a depth greater than 1 mm when the overlap ratio of the laser point is greater than the conventional one being processed. Constraints for in situ monitoring of the residual stress by employing LSP could be that LSP facilities are harder to integrate with existing industrial SLM machines, and LSP might prolong the printing time by a large extent.

5.4. Porosity

In general, porosity is a measure for estimating the level of hardness achieved in an additive manufactured metal sample. Porosity is a defect that appears as a pore or void, or in the absence of solid material in the turbine blades processed by AM. However, in some metal additive manufacturing techniques, a section of metal powder is melted with the help of a laser at the point where the powder bed melts and adheres to the previously melted layer. Sometimes complete fusion does not occur and results in the production of cavities in the blade, the final product, which is referred to as porosity [130]. Beyond a critical size (100 µm), porosity varies inversely with particle size. Therefore, to decrease the porosity, the laser power is regulated by considering the material's reflectivity and absorptivity. One of the laser process parameters (i.e., the laser scanning speed) can be used to adjust the type of pores generated during manufacturing and influence the energy density transferred to the powder bed during processing. Generally, the porosity (P) can be estimated from the measurement of density (ρ) using Equation (4) [131]:

$$P = \left(1 - \frac{\rho_{\text{measured}}}{\rho_{\text{theoretical}}} \right) \times 100 \quad (4)$$

where ρ_{measured} is the measured density of the part and $\rho_{\text{theoretical}}$ is the theoretical density of the fully dense material.

5.5. Roughness

The quality of the blade surface produced is of great concern for the aviation industry. This is due to the staircase effect observed on the blade surface, which is a consequence of the layer-by-layer nature of the manufacturing techniques. The representation of the staircase effect is shown in Figure 16. This phenomenon is concerning because it affects the dimensional accuracy and the surface roughness of the blade [132]. Surface roughness is a property that takes into account the presence of variation on the surface of an artifact. Not only does roughness play a role in the aesthetic part (e.g., shiny or matte), but it can also affect wear resistance, fatigue resistance, mating, sealing, rolling and fluid dynamics, and can act as crack initiation. Thus, there is a significant need for post-processing routes. Ultimately, this condition has a major influence on the overall production time and value

of production [133]. Equation (5) represents the arithmetic average of absolute values (S_a) that is used to estimate the roughness of SLM parts [134].

$$S_a = \frac{1}{A} \int_A Z(x,y) dx dy \tag{5}$$

where A is the number of points and $Z(x,y)$ defines the height of each point on the surface. Figure 16 shows the mean R_a for the structures that were printed using different AM techniques.

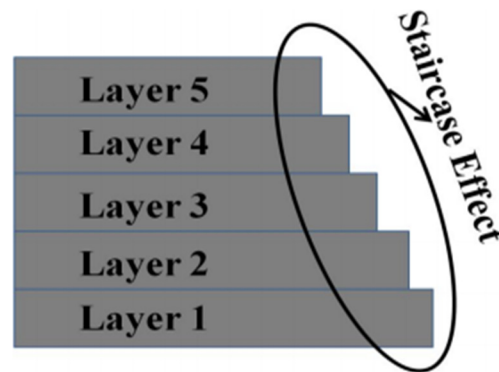


Figure 16. Schematic representation of the staircase effect in layer-based manufacturing.

In metal 3D printing, three main sources of surface roughness are listed [135,136]: first, lower process resolution and layering effects can cause the presence of surface artifacts; second, the presence of granular texture in the micro-surfaces from melting and adhesion in powder raw materials; and third, the presence of surface marks due to poor processing or removal of the support structures. Therefore, the following five categories of parameters are essential to determine the surface roughness after fabricating a 3D part, which are discussed below.

- (a) Core process resolution and precision: Resolution and accuracy are key parameters for 3D printing of the turbine blade and also to determine surface roughness. This is because 3D printing creates parts layer-by-layer and the resolution can be classified according to the axis. In the XY axes, the resolution depends on the processes that take place specifically in production [137]. For example, in PBF techniques, the diameter of the laser or electron beam is a measure of the resolution of the process while in binder jetting, the resolution of the jetting process is achieved in dots per inch (DPI). In the case of the DED technique, the width of the spheres deposited is the measure of the resolution. In the Z direction, the resolution for most processes is associated with the layer thickness or the slice thickness. The XY and Z resolutions of typical 3D printing processes are given in Table 3 [138]. When designing the component, viz., turbine blade, using AM, it is better for the designer to have an understanding of the part orientation and the build direction, so that they can decide the optimal number of features that will be subjected to high forces oriented in the X–Y plane.

Table 3. XY and Z axis resolutions of various 3D print processes [139].

Metal AM Process	Typical XY Resolution (μm)	Typical Z Resolution (μm)
Binder Jetting	20–65 (400–1200 DPI)	50–100
PBF	20–200	20–200
Powder DED	100–1000 (0.1–1 mm)	100–1000 (0.1–1 mm)

- (b) Material feedstock-type, size, and quality: Parameters such as the morphology of the powder particles (size and shape) and the quality of the powder present in the raw material influence the surface roughness. In PBF and binder jetting processes, the

physical properties of the powder grains such as the size and shape that are attached to the exterior side of the finished part have an impact on the roughness. Generally, raw powder materials can differ in shapes from spherical shapes with sizes as low as 5 μm, and unevenly shaped up to 120 μm particles. Here, the quality of the powder is a crucial parameter in processing as low-level powder can lead to undesirable mechanisms such as clumping, which prevents the powder from properly flowing and distributing, resulting in increased surface roughness [140].

- (c) **Print orientation:** The surface quality of blade fabricated using AM process is directly related to print orientation. The print orientation of the blade’s surface plays a crucial role [141]. The total printing height of the product is determined by the print orientation. As the height increases, the number of layers to be printed increases, which in turn increases the total vertical surfaces to be printed. Thus the staircase effect by every layer along the Z direction increases eventually, resulting in the poor surface finish of the blade.
- (d) **Support structure:** The use of support material is essential in most AM technologies. Supports are provided for the overhanging features of the part. Supports also assist in anchoring certain features to the build plate. Support material also takes part in heat transfer. The amount of support structures depends on the part orientation. Support material greatly affects surface quality and post-processing cost. These support structures are not part of the actual product and hence they are removed during post-processing. The physical removal of these support structures may lead to residual features left on the part, which also contributes to the surface roughness [142].
- (e) **Other key processing parameters:** The various processing parameters that can alter the surface roughness of the parts include power input, print speed, build geometry, and cooling rates. To obtain the highest surface quality, these parameters must be optimized as per the specific AM process [143].

Therefore, due to the nature of fabrication, post-processing is essential to adjust the surface roughness. Additionally, the fabrication of near-net-shape products generally creates parts that are very close to the final part and need secondary materials to remove and bring the sample down to its final specifications and smoothness [144]. The chart shown in Figure 17 is a comparison of the surface roughness produced by various additive manufacturing processes. Therefore, post-processing techniques are involved with specific techniques in the workflow of metal AM. The techniques for post-processing that are most widely accepted are CNC milling and turning, grinding, and polishing [145]. The standard fabricated part has a surface roughness of approximately ~3 μm. With an additional finish, the machining further reduced the surface roughness to ~1 μm [146].

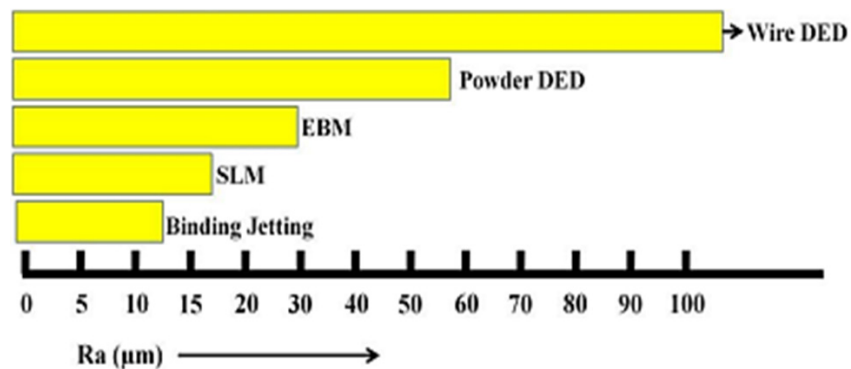


Figure 17. Comparison between the surface roughness produced by the various manufacturing processes [139].

A convenient technique such as abrasive fluid machining is used for parts where machining cannot be performed using CNC such as the internal surfaces of compliant cooling channels. In addition, there are convenient automated methods such as tumbling,

shot blasting, and centrifugation, which are often used on external surfaces. Conversely, the methods do not significantly improve surface roughness and further damage critical features and parts such as corners and edges [147]. The trigonometric formula proposed for the calculation of surface roughness with square angles and acute triangular angles are presented in Equations (6) and (7), respectively [148]:

$$R_a = \frac{t}{4} \cos(\theta) \quad (6)$$

$$R_a = \frac{\sum A^n}{L^n} = \frac{t(\tan \varphi \sin \theta + \cos \theta)}{4} + K \quad (7)$$

where R_a is the surface roughness; t is the layer thickness; φ is the angle counterclockwise from the vertical line; and θ is the surface angle or built orientation. For complex parts with high specifications with regard to surface roughness, the time consumed in post-processing could exceed the actual printing. The cost of production and time increases as more materials need to be machined from the printed parts. In AM, it is crucial to achieve a near-net-shape as any additional material will only contribute to making the final part more expensive due to high-cost material and energy waste [149,150].

6. Defect Formation, Cracking Mechanisms, and Strength

Currently, porosity, cracks, and multiple morphologies observed in the AM processed parts are the most common defects. The presence of certain types of defects depends on the AM technique used, the processing parameters involved in that technique, and the composition and morphology of raw material. Pore formation during the processing of turbine blade materials such as Ni-based super-alloys is largely induced due to processing and there is no significant difference in these observations, even with variable alloy compositions [151]. The consolidation threshold does not appear to depend on super-alloys because they show the evolution due to the incomplete consolidation of Ni-based super-alloys. While a consolidation threshold is also observed for Hastelloy-X material processed by direct laser deposition. Balling is another source for defect formation and it occurs due to discontinuous laser tracks and melt pools [152]. Presently, there are four cracking mechanisms observed in Ni-based super-alloys processed by AM techniques. These mechanisms include post-weld heat treatment cracking, cracking during solidification, liquation cracking, and ductility-dip cracking. Due to the rapid cooling during solidification, some liquid melt gets trapped between dendrites that have already solidified. Such zones will be present as weak zones at the end of solidification. Under the application of stress, the weak regions tend to rupture and tear, creating solidification cracks with jagged features. Solidification cracking also occurs though the application of higher energy densities during the fabrication process [153]. Interestingly, few studies have reported the contradictory result of a reduction in solidification cracking with the increase in energy density. Moreover, the size of the component also affects the onset of solidification cracking. With the increase in the size of the component, the thermal gradient increases result in solidification cracks. For example, the influence of Zr segregation on solidification cracking in IN738LC [154]. The study reported that the Zr films that are trapped between the dendritic arms close to the grain boundaries lead to the embrittlement of the grain-boundary region, resulting in cracks.

The fine grain structure resulting from AM techniques leads to an increase in the strength of the fabricated products. The refinement contributes toward improving the yield and ultimate tensile strength. The static strength of the materials varies depending on the obtained microstructure. The resultant microstructure depends on the combination of processing parameters and post-process heat treatment applied during fabrication [155]. The requirement of the heat treatment depends on the purpose of the part fabricated. As in the case of precipitation-hardened materials, the AM-produced products are soft in the absence of precipitations. The precipitates are not formed due to the rapid solidification and rather a fast cooling. Therefore, heat treatment could help the material reach maximum

strength in the peak-aged condition. With the presence of adequate heat treatments, a transformation in the microstructure of Ti-based turbine blade could lead to enhanced ductility. Along with other physical properties, the fatigue strength of the metallic product also depends on the microstructure, surface roughness, and presence of defects [156]. However, it was observed that mechanical surface treatments improve fatigue behavior. The mode of failure may be attributed to the presence of porosity. A ductile fracture will be observed when the porosity is low (0.1%), while a brittle fracture can be observed in the case of high porosity (2.4%) [157,158]. Besides, oxygen is one of a major factor influencing the strength and ductility of the AM processed product [159]. Treating porosities by densifying the material results in superior fatigue properties. The fatigue strength obtained in AM fabricated material is comparable to cast and wrought materials [160,161].

7. Microstructural Anisotropy

The Ni-based super-alloy parts processed by AM show substantial segregation in the inter-dendrites or unwanted phases (e.g., Laves phase) developed by solidification. Consequently, it raises the requirement of post-processing treatment, intending to remedy defects produced by AM processes [16]. The processing of materials through AM often results in a microstructure with a columnar grain structure, and this reaches up to several layers that are re-melted during processing. During printing, the layer of material is often heated and cooled multiple times, resulting in microstructural inhomogeneity on a micrometer scale, generally known as “fish-scale” morphology (Figure 18a), the segregation into inhomogeneous grain structures. Anisotropy in grain structure is not necessarily the problem as these anisotropies are employed to tailor mechanical properties for specific applications. The metastable nature of rapid solidification is a challenge for the additive manufacturing process. The rapid solidification leads to the epitaxial growth of the microstructure (Figure 18b), which is generally observed in the PBF and DED processes, whereas in the case of the SLS process, nearly equiaxial grain regions are observed replacing the columnar grains, as shown in Figure 18c, which is because of the scanning strategy employed in SLS. With the chessboard scanning strategy, the laser moves randomly between square islands to distribute the heat, evenly resulting in equiaxial grain growth [116]. Recently, studies have revealed the ability of AM to control grain-size and crystal orientation by controlling its process parameters [162]. Most of the microstructural changes on the printed surface have not been revealed. Hence, both microstructural and texture need to be investigated.

By manipulating the cooling profile, columnar grain growth can be avoided in the case of the direct laser deposition technique. Microstructural engineering and texture require further research from the AM community.

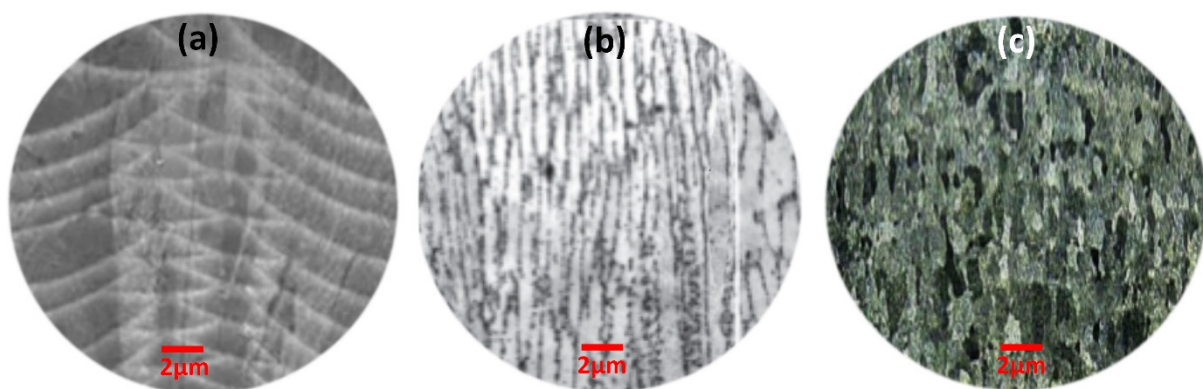


Figure 18. (a) Fish-scale morphology due to repeated heating and cooling, (b) epitaxial growth of the microstructure as observed in DED, and (c) equiaxial grain regions found in SLM.

8. Summary and Future Perspective

Achieving changes in processing, design, weight, shape, strength, and performance of the blade leads to a significant contribution to the overall performance of jet engines and hence to the aviation industry. In this regard, the manuscript has explicated the insights into the additive manufacturing (AM) of turbine blades. Gradual development of turbine blades was elaborated here to understand the traditional turbine blade design along with advanced designs such as AM. The applicable AM techniques such as SLM, SLS, EBM, aerosol jet, binder jet, LENS, EBF3, and laser cladding for the processing of gas turbine blades have been discussed in detail. On the other hand, the change in the internal cooling systems of the turbine blade influenced by the application of DFAM techniques has also been represented here to understand the complexity and how the AM process simplifies the complexity. The design flexibility of AM further reduces the cost and weight of the components as well as the development of the most complex internal geometry of turbine blades. Advanced monitoring techniques employed on the turbine blades by integrating sensors on the blade surfaces using AM techniques have also been elucidated. The current state-of-the-art of the implementation of AM for turbine blade fabrication by the leading companies in the aviation industries is elaborated here. The use of AM techniques provides opportunities to incorporate complex and flexible designs with a reduction in production steps. The effect of various operating parameters on the turbine blade has been described. Along with the techniques for the fabrication of turbine blades, the manuscript also presents a few other techniques of AM that are used for the repair of turbine blades. Although advancements in the processing of turbine blades using AM have been made, however, there is huge scope for improvement in terms of design, newer materials, processing method, newer controlling and monitoring of process parameters, mechanical properties, and the overall quality of the turbine blade. This opens the way for more research and development necessary to annihilate several in situ defects in products processed by AM.

Author Contributions: Conceptualization, A.B. (Ajit Behera); methodology, A.B. (Ajit Behera); formal analysis, A.B. (Asit Behera), H.M.V.; investigation, B.S.; P.M.; resources, A.B. (Ayush Sinha); A.B. (Asit Behera); data curation, A.B. (Asit Behera); S.K.S.; writing—original draft preparation, A.S. writing—review and editing, A.B. (Ajit Behera); H.M.V.; visualization, A.B. (Ajit Behera); supervision, A.B. (Ajit Behera). All authors have read and agreed to the published version of the manuscript.

Funding: This research received no external funding.

Data Availability Statement: Not applicable.

Conflicts of Interest: The authors declare no conflict of interest.

References

- Verde, C.; Sánchez-Parra, M. Monitorability Analysis for a Gas Turbine Using Structural Analysis. In *Fault Detection, Supervision and Safety of Technical Processes 2006*; Elsevier: Amsterdam, The Netherlands, 2007; pp. 675–680.
- Pattnaik, S.; Karunakar, D.B.; Jha, P.K. Developments in Investment Casting Process—A Review. *J. Mater. Process. Technol.* **2012**, *212*, 2332–2348. [[CrossRef](#)]
- EOS Turbine Blade. Available online: <https://www.eos.info/en/3d-printing-examples-applications/production-and-industry/turbomachinery-turbines> (accessed on 15 November 2021).
- Jiang, R.; Kleer, R.; Piller, F.T. Predicting the Future of Additive Manufacturing: A Delphi Study on Economic and Societal Implications of 3D Printing for 2030. *Technol. Forecast. Soc. Chang.* **2017**, *117*, 84–97. [[CrossRef](#)]
- Richardson, J.J.; Cui, J.; Björnalm, M.; Braunger, J.A.; Ejima, H.; Caruso, F. Innovation in Layer-by-Layer Assembly. *Chem. Rev.* **2016**, *116*, 14828–14867. [[CrossRef](#)] [[PubMed](#)]
- Turbine Blade 1c. Available online: https://www.wikiwand.com/en/Turbine_blade (accessed on 15 November 2021).
- Magerramova, L.; Vasilyev, B.; Kinzburskiy, V. Novel Designs of Turbine Blades for Additive Manufacturing. In Proceedings of the ASME Turbo Expo 2016: Turbomachinery Technical Conference and Exposition, Seoul, Korea, 13–17 June 2016.
- Additive Manufacturing Market. Available online: <https://www.researchcosmos.com/reports/additive-manufacturing-market/1170635782> (accessed on 15 November 2021).
- GE Aviation Invests in Widespread Rollout of GE Additive Arcam EBM Technology to Support GE9X Blade Production. Available online: <https://www.ge.com/additive/press-releases/ge-aviation-invests-widespread-rollout-ge-additive-arcam-ebm-technology-support-ge9x> (accessed on 15 November 2021).

10. Angel, N.M.; Basak, A. On the Fabrication of Metallic Single Crystal Turbine Blades with a Commentary on Repair via Additive Manufacturing. *J. Manuf. Mater. Process.* **2020**, *4*, 101. [[CrossRef](#)]
11. Lattime, S.; Steinetz, B. Turbine Engine Clearance Control Systems: Current Practices and Future Directions. In Proceedings of the 38th AIAA/ASME/SAE/ASEE Joint Propulsion Conference & Exhibit, Indianapolis, Indiana, 7–10 July 2002.
12. Chatterjee, B.; Bhowmik, S. Chapter 9—Evolution of Material Selection in Commercial Aviation Industry—A Review. In *Sustainable Engineering Products and Manufacturing Technologies*; Academic Press: Cambridge, MA, USA, 2019; pp. 199–219. ISBN 978-0-12-816564-5. [[CrossRef](#)]
13. GE9X Commercial Aircraft Engine | GE Aviation. Available online: <https://www.geaviation.com/commercial/engines/ge9x-commercial-aircraft-engine> (accessed on 15 November 2021).
14. Aircraft Engine Blades Market—Growth, Trends, Covid-19 Impact, and Forecasts (2022–2027). Available online: <https://www.mordorintelligence.com/industry-reports/aircraft-engine-blades-market> (accessed on 15 November 2021).
15. M88—Proven Performance and Reliability. Available online: <https://www.safran-aircraft-engines.com/military-engines/training-and-combat-aircraft/m88> (accessed on 15 November 2021).
16. Mertens, A.I.; Delahaye, J.; Lecomte-Beckers, J. Fusion-Based Additive Manufacturing for Processing Aluminum Alloys: State-of-the-Art and Challenges. *Adv. Eng. Mater.* **2017**, *19*, 1700003. [[CrossRef](#)]
17. Singh, K. Advanced Materials for Land Based Gas Turbines. *Trans. Indian Inst. Met.* **2014**, *67*, 601–615. [[CrossRef](#)]
18. Langston, L.S. Powering Out of Trouble. *Mech. Eng.* **2013**, *135*, 36–41. [[CrossRef](#)]
19. Wang, T. 15—The Gas and Steam Turbines and Combined Cycle in IGCC Systems. In *Integrated Gasification Combined Cycle (IGCC) Technologies*; Elsevier: Amsterdam, The Netherlands, 2017; pp. 497–640. ISBN 978-0-08-100167-7. [[CrossRef](#)]
20. Chyu, M.K.; Siw, S.C. Recent Advances of Internal Cooling Techniques for Gas Turbine Airfoils. *J. Therm. Sci. Eng. Appl.* **2013**, *5*, 2–12. [[CrossRef](#)]
21. Turbine Blade Internal Cooling. Available online: https://www.wikiwand.com/en/Turbine_blade (accessed on 15 November 2021).
22. Koff, B.L. Gas Turbine Technology Evolution: A Designers Perspective. *J. Propuls. Power* **2004**, *20*, 577–595. [[CrossRef](#)]
23. Dai, S.; Xiao, Y.; He, L.; Jin, T.; Hou, P.; Zhang, Q.; Zhao, Z. Computational Study of Plasma Actuator on Film Cooling Performance for Different Shaped Holes. *AIP Adv.* **2015**, *5*, 67104. [[CrossRef](#)]
24. Turbine Blade External Cooling. Available online: https://en.wikipedia.org/wiki/Turbine_blade (accessed on 15 November 2021).
25. Blading, W.C. Variable Camber Blading. Patent U.S. 3042371, 3 July 1962.
26. Suter, D.P. Blading for Rotors of Axial Compressors 1969. Patent DE1903642A1, 8 June 1969.
27. Ziegler, G.D.I. Twisted and Tapered Blade for Axial Turbo Machinery. Patent DE2144600A1, 15 March 1973.
28. Brown, R. Guide Vanes for Supersonic Turbine Blades 1974. Patent U.S. 3837761A, 24 September 1974.
29. Bliss, D.B. Method of and Apparatus for Preventing Leading Edge Shocks and Shock-Related Noise in Transonic and Supersonic Rotor Blades and the Like 1976. Patent U.S. 3989406A, 2 November 1976.
30. Kazin, S.B.; Matta, R.K. Curved Blade Turbomachinery Noise Reduction 1978. Patent U.S. 4131387A, 26 December 1978.
31. Zipps, R.H.; Rynaski, C.H.; Fulton, G.B. Fan Rotor Blades of Turbofan Engines 1986. Patent U.S. 4621979A, 11 November 1986.
32. Application filed by United Technologies Corp Rotor Assembly for Gas Turbine Engine 1982. Patent IL67806A, 31 October 1986.
33. Martin, J.R. Bowed Turbine Blade 1987. Patent U.S. 4682935A, 28 July 1987.
34. Braddy, B.T.; Eldrid, S.Q. Turbine Blade with Tip Vent 1988. Patent U.S. 4761116A, 2 August 1988.
35. Brent, A. Gregory Curvilinear Turbine Airfoil 1986. Patent U.S. 4826400A, 2 May 1989.
36. Wertz, T.A.; Saltzman, G.A.; Friedman, I.L. Turbine Blade with Restored Tip 1989. Patent U.S. 4808055A, 28 February 1989.
37. Mank, H. Tran Free Standing Blade for Use in Low Pressure Steam Turbine 1991. Patent U.S. 5017091A, 21 May 1991.
38. John, W. Magowan Coolable Rotor Blade Structure 1994. Patent WO1994012390A2, 9 June 1994.
39. Jurek, F.; Daniel, R. Cornell Light Weight Steam Turbine Blade 1993. Patent U.S. 5352092A, 4 October 1994.
40. Lee, C.P.; Pietraszkiewicz, E.F.; Prakash, C.; Zerkle, R.D. Turbine Blade Having Tip Slot 1996. Patent U.S. 5503527A, 2 April 1996.
41. Thomas, A.; Frank, W.; HuberRobert, R.; SellersFriedrich, O. Soechting Cooled Blades for a Gas Turbine Engine 1990. Patent AU684039B1, 4 December 1997.
42. Norbert, H.; Reinhard, D. Niehuis Turbomachine Blade 1997. Patent EP0798447B1, 5 September 2001.
43. Auxier, T.; Hall, K.; McClelland, R. Cooled Blades for a Gas Turbine Engine 1988. Patent AU684037B1, 4 December 1997.
44. Take Sato, Y.Y. Axial Flow Turbine Vane Device and Axial Flow Turbine 1990. Patent JP2753382B2, 20 May 1998.
45. Pepperman, L.; Pepperman, B. Gas Turbine Blade with Cooled Platform 1998. Patent EP0777818B1, 14 October 1998.
46. Rowlands, P.A. Swept Fan Blade 2000. Patent U.S. 6071077A, 6 June 2000.
47. Wood, P.; Decker, J.; Steinmetz, T.; Mielke, M.; Seitzer, K. Narrow Waist Vane 2001. Patent U.S. 6312219B1, 6 November 2001.
48. Bauer, K. Helicopter Rotor Blade with a Movable Flap 2001. Patent U.S. 6168379B1, 2 January 2001.
49. Chandraker, A. Three Dimensional Blade 2004. Patent U.S. 20030086788A1, 23 March 2004.
50. Ganshaw, T.J. Stress Relieved Blade Support 2001. Patent U.S. 6183202B1, 6 February 2001.
51. Goodman, P.J. Tip Sealing for a Turbine Rotor Blade 2006. Patent GB2409006B, 17 May 2006.
52. Bagai, A. Rotor Blade Pitch Control Assembly 2006. Patent U.S. 6984109B2, 10 January 2006.
53. Richard, S.; Chiurato, R. Turbine Blade Pocket Shroud 2001. Patent CN100351495C, 28 November 2007.
54. Takahashi, C.M. Transonic Blade 2010. Patent U.S. 20100215503A1, 23 April 2013.

55. Sun, F.; Chaudhry, Z.; Yeh, J.; O'Callaghan, M.; Jonsson, U.; Wake, B.; Dold, R. Hybrid Actuator for Helicopter Rotor Blade Control Flaps 2008. Patent U.S. 7762770B2, 27 July 2010.
56. Wood, P.; Falk, E.; Dailey, L. Advanced Booster Rotor Blade 2011. Patent U.S. 7967571B2, 28 June 2011.
57. Kilaras, M.S. Vortex Dynamics Turbine 2011. Patent U.S. 20110229321A1, 22 September 2011.
58. Fred, T.; Willett, J. Turbines and Turbine Blade Winglets 2013. Patent U.S. 8414265B2, 9 April 2013.
59. Suciu, G.L.; James, D.H.; Gary, M.S. Reverse Cavity Blade for a Gas Turbine Engine 2010. Patent U.S. 8740567B2, 3 June 2014.
60. Penny, C.; Gustafson, R. Turbomachine Blade with Tip Flare 2013. Patent U.S. 8894376B2, 25 November 2014.
61. Hoebel, M.; Ambrosy, G.; Reinert, F.; Barril, S. Wear-Resistant and Oxidation-Resistant Turbine Blade 2015. Patent EP2316988B1, 8 July 2015.
62. Chouhan, R.; Bommanakatte, H.; Soni, S.; Jayana, S.G.; Kareff, S.A. Fillet for Use with a Turbine Rotor Blade Tip Shroud 2014. Patent U.S. 9322282B2, 26 April 2016.
63. Wunderer, R. Blade Cascade and Turbomachine 2013. Patent U.S. 9404368B2, 2 August 2016.
64. Craig, K.; Joseph, B.; Alisha, K. Turbine Blade with Contoured Platform 2011. Patent CA2771349C, 5 September 2017.
65. Jones, M.A.; Brozyna, L.L. Turbine Blade Centroid Shifting Method and System 2017. Patent U.S. 9995144B2, 12 June 2018.
66. Man, M.D.; Delabrierel, P.; Coudert, J.-A.M.; Destouches, M. Optimized Aerodynamic Profile for a Turbine Vane, in Particular for a Nozzle of the Second Stage of a Turbine 2018. Patent U.S. 10443392B2, 15 October 2019.
67. Hamed, A.A.; Tabakoff, W.; Rivir, R.B.; Das, K.; Arora, P. Turbine Blade Surface Deterioration by Erosion. *J. Turbomach.* **2004**, *127*, 445–452. [[CrossRef](#)]
68. Ruffles, P.C. Aero Engines of the Future. *Aeronaut. J.* **2003**, *107*, 307–321. [[CrossRef](#)]
69. Wei, Z.; Qiao, W.; Shi, P.; Chen, P.; Zhao, L. Tip-Leakage Flow Loss Reduction in a Two-Stage Turbine Using Axisymmetric-Casing Contouring. *Chin. J. Aeronaut.* **2014**, *27*, 1111–1121. [[CrossRef](#)]
70. Turbine Cooling Trent 500. Available online: <https://aerospaceengineeringblog.com/turbine-cooling/> (accessed on 15 November 2021).
71. Pal, A.; Bertoldi, K.; Pham, M.Q.; Schaenzer, M.; Gross, A.J. Optimal Turbine Blade Design Enabled by Auxetic Honeycomb. *Smart Mater. Struct.* **2020**, *29*, 125004. [[CrossRef](#)]
72. Garg, S. Aircraft Turbine Engine Control Research at NASA Glenn Research Center. *J. Aerosp. Eng.* **2013**, *26*, 422–438. [[CrossRef](#)]
73. Xue, S.; Ng, W.F. Turbine Blade Tip External Cooling Technologies. *Aerospace* **2018**, *5*, 90. [[CrossRef](#)]
74. Schubel, P.J.; Crossley, R.J. Wind Turbine Blade Design. *Energies* **2012**, *5*, 3425–3449. [[CrossRef](#)]
75. Matsuura, K.M.K. 3D Free Shaping Method and 3D Free Shaping Apparatus. Patent JP4223637B2, 12 February 2009.
76. Jennings, C. Gas Turbine Engine Component Having Engineered Vascular Structure. Patent EP3179042B1, 4 March 2020.
77. Xu, J. Method for Forming Components Using Additive Manufacturing and Re-Melt. Patent U.S. 20160339516A1, 1 August 2017.
78. Garner, C. Turbine Blade Having an Additive Manufacturing Trailing Edge. Patent U.S. 20190063229A1, 2 March 2021.
79. Tapia, L.; Halfmann, S.; Harman, S.A. Turbine Rotor Assemblies with Improved Slot Cavities. Patent EP2896786B1, 13 March 2019.
80. Thomas, S.; Mironets, A.; Staroselsky, B.S.; Thomas, M. Airfoil, and Method for Manufacturing the Same. Patent U.S. 20160369634A1, 26 November 2019.
81. Tracy, H.; Dominic, M.; Benjamin, F. Additively Manufactured Core. Patent 10525525, 7 January 2020.
82. Kruth, J.P.; Wang, X.; Laoui, T.; Froyen, L. Lasers and Materials in Selective Laser Sintering. *Assem. Autom.* **2003**, *23*, 357–371. [[CrossRef](#)]
83. Yap, C.Y.; Chua, C.K.; Dong, Z.L.; Liu, Z.H.; Zhang, D.Q.; Loh, L.E.; Sing, S.L. Review of Selective Laser Melting: Materials and Applications. *Appl. Phys. Rev.* **2015**, *2*, 041101. [[CrossRef](#)]
84. Additive Manufacturing: Siemens Uses Innovative Technology to Produce Gas Turbines. Available online: <https://press.siemens.com/global/en/feature/additive-manufacturing-siemens-uses-innovative-technology-produce-gas-turbines> (accessed on 15 November 2021).
85. Simens Ni Alloy Based Turbine Blade. Available online: <https://blogs.sw.siemens.com/nx-design/3d-printing-in-nx/> (accessed on 15 November 2021).
86. Galati, M.; Iuliano, L. A Literature Review of Powder-Based Electron Beam Melting Focusing on Numerical Simulations. *Addit. Manuf.* **2018**, *19*, 1–20. [[CrossRef](#)]
87. Rafi, H.K.; Karthik, N.V.; Gong, H.; Starr, T.L.; Stucker, B.E. Microstructures and Mechanical Properties of Ti6Al4V Parts Fabricated by Selective Laser Melting and Electron Beam Melting. *J. Mater. Eng. Perform.* **2013**, *22*, 3872–3883. [[CrossRef](#)]
88. EBM Made Turbine Blade by GE. Available online: <https://www.ge.com/additive/stories/additive-at-scale-avio-aero> (accessed on 15 November 2021).
89. Kellner, T. Avio Aero, a General Electric (GE) Aviation EBM Turbine Blade. Available online: <https://www.ge.com/news/reports/future-manufacturing-take-look-inside-factory-3d-printing-jet-engine-parts> (accessed on 15 November 2021).
90. Yadav, P.; Fu, Z.; Knorr, M.; Travitzky, N. Binder Jetting 3D Printing of Titanium Aluminides Based Materials: A Feasibility Study. *Adv. Eng. Mater.* **2020**, *22*, 2000408. [[CrossRef](#)]
91. Mostafaei, A.; Stevens, E.L.; Hughes, E.T.; Biery, S.D.; Hilla, C.; Chmielus, M. Powder Bed Binder Jet Printed Alloy 625: Densification, Microstructure and Mechanical Properties. *Mater. Des.* **2016**, *108*, 126–135. [[CrossRef](#)]
92. Popov, V.V.; Grilli, M.L.; Koptuyg, A.; Jaworska, L.; Katz-Demyanetz, A.; Klobčar, D.; Balos, S.; Postolnyi, B.O.; Goel, S. Powder Bed Fusion Additive Manufacturing Using Critical Raw Materials: A Review. *Materials* **2021**, *14*, 909. [[CrossRef](#)]

93. Varotsis, A.B. Introduction to Binder Jetting 3D Printing- 3D HUBS. Available online: <https://www.hubs.com/knowledge-base/introduction-binder-jetting-3d-printing/> (accessed on 15 November 2021).
94. Everett, H. Exone to Develop High-Strength Steel Alloy for U.S. Air Force—3d Printing Industry. Available online: <https://3dprintingindustry.com/news/exone-to-develop-high-strength-steel-alloy-for-u-s-air-force-177992/> (accessed on 15 November 2021).
95. Fang, X.; Du, J.; Wei, Z.; He, P.; Bai, H.; Wang, X.; Lu, B. An Investigation on Effects of Process Parameters in Fused-Coating Based Metal Additive Manufacturing. *J. Manuf. Process.* **2017**, *28*, 383–389. [CrossRef]
96. Eboo, G.M.; Blake, A.G. Laser Cladding of Gas Turbine Components. In Proceedings of the ASME 1986 International Gas Turbine Conference and Exhibit, Dusseldorf, Germany, 8–12 June 1986. [CrossRef]
97. Alimardani, M.; Fallah, V.; Khajepour, A.; Toyserkani, E. The Effect of Localized Dynamic Surface Preheating in Laser Cladding of Stellite 1. *Surf. Coatings Technol.* **2010**, *204*, 3911–3919. [CrossRef]
98. Izadi, M.; Farzaneh, A.; Mohammed, M.; Gibson, I.; Rolfe, B. A Review of Laser Engineered Net Shaping (LENS) Build and Process Parameters of Metallic Parts. *Rapid Prototyp. J.* **2020**, *26*, 1059–1078. [CrossRef]
99. Vaezi, M.; Chianrabutra, S.; Mellor, B.; Yang, S. Multiple Material Additive Manufacturing—Part 1: A Review. *Virtual Phys. Prototyp.* **2013**, *8*, 19–50. [CrossRef]
100. Albuquerque Optomec Customers Surpass 10 Million Turbine Blade Repairs. Available online: <https://optomec.com/optomec-customers-surpass-10-million-turbine-blade-repairs/> (accessed on 15 November 2021).
101. Carlota, V. Optomec Customers Have Repaired More than 10 Million Turbine Blades- Optomec. Available online: <https://www.3dnatives.com/en/optomec-customer-surpass-10-million-turbine-blade-repairs-260820204/#!> (accessed on 15 November 2021).
102. Majumdar, T.; Eisenstein, N.; Frith, J.E.; Cox, S.C.; Birbilis, N. Additive Manufacturing of Titanium Alloys for Orthopedic Applications: A Materials Science Viewpoint. *Adv. Eng. Mater.* **2018**, *20*, 1800172. [CrossRef]
103. William, J.; Seufzer Robert, A. Hafley Height Control and Deposition Measurement for the Electron Beam Free Form Fabrication (EBF3) Process. Patent 9764415, 19 September 2017.
104. Electron-Beam Freeform Fabrication (EBF3): Technology and Application. Available online: <https://3d-expo.ru/en/article/proizvodstvo-elektronno-luchevoy-plavkoy-ebf-tehnologiya-i-primenenie-80098> (accessed on 15 November 2021).
105. AMFG Application Spotlight: 3D Printing for Turbine Parts. Available online: <https://amfg.ai/2020/02/06/application-spotlight-3d-printing-for-turbine-parts/> (accessed on 15 November 2021).
106. Reitberger, T.; Hoerber, J.; Schramm, R.; Sennefelder, S.; Franke, J. Aerosol Jet[®] Printing of Optical Waveguides. In Proceedings of the 2015 38th International Spring Seminar on Electronics Technology (ISSE), Eger, Hungary, 6–10 May 2015. [CrossRef]
107. Garboczi, E.J.; Hrabe, N. Particle Shape and Size Analysis for Metal Powders Used for Additive Manufacturing: Technique Description and Application to Two Gas-Atomized and Plasma-Atomized Ti64 Powders. *Addit. Manuf.* **2020**, *31*, 100965. [CrossRef]
108. Strondl, A.; Lyckfeldt, O.; Brodin, H.; Ackelid, U. Characterization and Control of Powder Properties for Additive Manufacturing. *JOM* **2015**, *67*, 549–554. [CrossRef]
109. Bai, Y.; Wagner, G.; Williams, C.B. Effect of Particle Size Distribution on Powder Packing and Sintering in Binder Jetting Additive Manufacturing of Metals. *J. Manuf. Sci. Eng.* **2017**, *139*, 081019. [CrossRef]
110. Brika, S.E.; Letenneur, M.; Dion, C.A.; Brailovski, V. Influence of Particle Morphology and Size Distribution on the Powder Flowability and Laser Powder Bed Fusion Manufacturability of Ti-6Al-4V Alloy. *Addit. Manuf.* **2020**, *31*, 1–37. [CrossRef]
111. Kiani, P.; Scipioni Bertoli, U.; Dupuy, A.D.; Ma, K.; Schoenung, J.M. A Statistical Analysis of Powder Flowability in Metal Additive Manufacturing. *Adv. Eng. Mater.* **2020**, *22*, 2000022. [CrossRef]
112. Ali, U.; Mahmoodkhani, Y.; Imani Shahabad, S.; Esmailizadeh, R.; Liravi, F.; Sheydaeian, E.; Huang, K.Y.; Marzbanrad, E.; Vlasea, M.; Toyserkani, E. On the Measurement of Relative Powder-Bed Compaction Density in Powder-Bed Additive Manufacturing Processes. *Mater. Des.* **2018**, *155*, 495–501. [CrossRef]
113. Nguyen, Q.B.; Nai, M.L.S.; Zhu, Z.; Sun, C.-N.; Wei, J.; Zhou, W. Characteristics of Inconel Powders for Powder-Bed Additive Manufacturing. *Engineering* **2017**, *3*, 695–700. [CrossRef]
114. Spierings, A.B.; Schneider, M.; Eggenberger, R. Comparison of Density Measurement Techniques for Additive Manufactured Metallic Parts. *Rapid Prototyp. J.* **2011**, *17*, 380–386. [CrossRef]
115. Kamath, C.; El-dasher, B.; Gallegos, G.F.; King, W.E.; Sisto, A. Density of Additively-Manufactured, 316L SS Parts Using Laser Powder-Bed Fusion at Powers up to 400 W. *Int. J. Adv. Manuf. Technol.* **2014**, *74*, 65–78. [CrossRef]
116. Vickers, N.J. Animal Communication: When I’m Calling You, Will You Answer Too? *Curr. Biol.* **2017**, *27*, R713–R715. [CrossRef] [PubMed]
117. Micromeritics AccuPyc II. Available online: <https://www.micromeritics.com/accupyc-ii/> (accessed on 15 November 2021).
118. Micromeritics GeoPyc 1365. Available online: <https://www.micromeritics.com/micromeritics-geopyc-1365-envelope-density-analyzer/> (accessed on 15 November 2021).
119. Mussatto, A.; Groarke, R.; O’Neill, A.; Obeidi, M.A.; Delaure, Y.; Brabazon, D. Influences of Powder Morphology and Spreading Parameters on the Powder Bed Topography Uniformity in Powder Bed Fusion Metal Additive Manufacturing. *Addit. Manuf.* **2021**, *38*, 101807. [CrossRef]
120. Maamoun, A.H.; Xue, Y.F.; Elbestawi, M.A.; Veldhuis, S.C. Effect of Selective Laser Melting Process Parameters on the Quality of Al Alloy Parts: Powder Characterization, Density, Surface Roughness, and Dimensional Accuracy. *Materials* **2018**, *11*, 12. [CrossRef] [PubMed]

121. Khairallah, S.A.; Anderson, A.T.; Rubenchik, A.; King, W.E. Laser Powder-Bed Fusion Additive Manufacturing: Physics of Complex Melt Flow and Formation Mechanisms of Pores, Spatter, and Denudation Zones. *Acta Mater.* **2016**, *108*, 36–45. [CrossRef]
122. Li, C.; Liu, Z.Y.; Fang, X.Y.; Guo, Y.B. Residual Stress in Metal Additive Manufacturing. *Procedia CIRP* **2018**, *71*, 348–353. [CrossRef]
123. Megahed, M.; Mindt, H.-W.; N'Dri, N.; Duan, H.; Desmaison, O. Metal Additive-Manufacturing Process and Residual Stress Modeling. *Integr. Mater. Manuf. Innov.* **2016**, *5*, 61–93. [CrossRef]
124. Genzel, C.; Denks, I.A.; Gibmeier, J.; Klaus, M.; Wagener, G. The Materials Science Synchrotron Beamline EDDI for Energy-Dispersive Diffraction Analysis. *Nucl. Instrum. Methods Phys. Res. Sect. A Accel. Spectrometers Detect. Assoc. Equip.* **2007**, *578*, 23–33. [CrossRef]
125. Mishurova, T.; Artzt, K.; Haubrich, J.; Requena, G.; Bruno, G. Exploring the Correlation between Subsurface Residual Stresses and Manufacturing Parameters in Laser Powder Bed Fused Ti-6Al-4V. *Metals* **2019**, *9*, 261. [CrossRef]
126. Nadammal, N.; Mishurova, T.; Fritsch, T.; Serrano-Munoz, I.; Kromm, A.; Haberland, C.; Portella, P.D.; Bruno, G. Critical Role of Scan Strategies on the Development of Microstructure, Texture, and Residual Stresses during Laser Powder Bed Fusion Additive Manufacturing. *Addit. Manuf.* **2021**, *38*, 1–33. [CrossRef]
127. Mukherjee, T.; Zhang, W.; DebRoy, T. An Improved Prediction of Residual Stresses and Distortion in Additive Manufacturing. *Comput. Mater. Sci.* **2017**, *126*, 360–372. [CrossRef]
128. Szost, B.A.; Terzi, S.; Martina, F.; Boisselier, D.; Prytuliak, A.; Pirling, T.; Hofmann, M.; Jarvis, D.J. A Comparative Study of Additive Manufacturing Techniques: Residual Stress and Microstructural Analysis of CLAD and WAAM Printed Ti-6Al-4V Components. *Mater. Des.* **2016**, *89*, 559–567. [CrossRef]
129. Vastola, G.; Zhang, G.; Pei, Q.X.; Zhang, Y.-W. Controlling of Residual Stress in Additive Manufacturing of Ti6Al4V by Finite Element Modeling. *Addit. Manuf.* **2016**, *12*, 231–239. [CrossRef]
130. DePond, P.J.; Guss, G.; Ly, S.; Calta, N.P.; Deane, D.; Khairallah, S.; Matthews, M.J. In Situ Measurements of Layer Roughness during Laser Powder Bed Fusion Additive Manufacturing Using Low Coherence Scanning Interferometry. *Mater. Des.* **2018**, *154*, 347–359. [CrossRef]
131. Tapia, G.; Elwany, A.H.; Sang, H. Prediction of Porosity in Metal-Based Additive Manufacturing Using Spatial Gaussian Process Models. *Addit. Manuf.* **2016**, *12*, 282–290. [CrossRef]
132. Baturynska, I. Statistical Analysis of Dimensional Accuracy in Additive Manufacturing Considering STL Model Properties. *Int. J. Adv. Manuf. Technol.* **2018**, *97*, 2835–2849. [CrossRef]
133. Huang, S.H.; Liu, P.; Mokasdar, A.; Hou, L. Additive Manufacturing and Its Societal Impact: A Literature Review. *Int. J. Adv. Manuf. Technol.* **2013**, *67*, 1191–1203. [CrossRef]
134. Delgado, J.; Ciurana, J.; Rodríguez, C.A. Influence of Process Parameters on Part Quality and Mechanical Properties for DMLS and SLM with Iron-Based Materials. *Int. J. Adv. Manuf. Technol.* **2012**, *60*, 601–610. [CrossRef]
135. Jamshidinia, M.; Kovacevic, R. The Influence of Heat Accumulation on the Surface Roughness in Powder-Bed Additive Manufacturing. *Surf. Topogr. Metrol. Prop.* **2015**, *3*, 014003. [CrossRef]
136. Li, Z.; Zhang, Z.; Shi, J.; Wu, D. Prediction of Surface Roughness in Extrusion-Based Additive Manufacturing with Machine Learning. *Robot. Comput. Integr. Manuf.* **2019**, *57*, 488–495. [CrossRef]
137. Hirsch, M.; Patel, R.; Li, W.; Guan, G.; Leach, R.K.; Sharples, S.D.; Clare, A.T. Assessing the Capability of In-Situ Nondestructive Analysis during Layer Based Additive Manufacture. *Addit. Manuf.* **2017**, *13*, 135–142. [CrossRef]
138. Popov, D.; Maltsev, E.; Fryazinov, O.; Pasko, A.; Akhatov, I. Efficient Contouring of Functionally Represented Objects for Additive Manufacturing. *Comput. Des.* **2020**, *129*, 102917. [CrossRef]
139. Huckstepp, A. Surface Roughness—A Guide to Metal Additive Manufacturing by Digital Alloys. Available online: <https://manufactur3dmag.com/surface-roughness-a-guide-to-metal-additive-manufacturing-by-digital-alloys/> (accessed on 15 November 2021).
140. Bourell, D.; Kruth, J.P.; Leu, M.; Levy, G.; Rosen, D.; Beese, A.M.; Clare, A. Materials for Additive Manufacturing. *CIRP Ann.* **2017**, *66*, 659–681. [CrossRef]
141. Chowdhury, S.; Mhapsekar, K.; Anand, S. Part Build Orientation Optimization and Neural Network-Based Geometry Compensation for Additive Manufacturing Process. *J. Manuf. Sci. Eng.* **2017**, *140*, 031009. [CrossRef]
142. Higueros, E.; Roe, E.; Granell, E.; Baselga, E. Sturge-Weber Syndrome: A Review. *Actas Dermosifiliogr.* **2017**, *108*, 407–417. [CrossRef]
143. DebRoy, T.; Wei, H.L.; Zuback, J.S.; Mukherjee, T.; Elmer, J.W.; Milewski, J.O.; Beese, A.M.; Wilson-Heid, A.; De, A.; Zhang, W. Additive Manufacturing of Metallic Components—Process, Structure and Properties. *Prog. Mater. Sci.* **2018**, *92*, 112–224. [CrossRef]
144. Mukherjee, T.; Wei, H.L.; De, A.; DebRoy, T. Heat and Fluid Flow in Additive Manufacturing—Part II: Powder Bed Fusion of Stainless Steel, and Titanium, Nickel and Aluminum Base Alloys. *Comput. Mater. Sci.* **2018**, *150*, 369–380. [CrossRef]
145. Knapp, G.L.; Mukherjee, T.; Zuback, J.S.; Wei, H.L.; Palmer, T.A.; De, A.; DebRoy, T. Building Blocks for a Digital Twin of Additive Manufacturing. *Acta Mater.* **2017**, *135*, 390–399. [CrossRef]
146. Yin, S.; Cavaliere, P.; Aldwell, B.; Jenkins, R.; Liao, H.; Li, W.; Lupoi, R. Cold Spray Additive Manufacturing and Repair: Fundamentals and Applications. *Addit. Manuf.* **2018**, *21*, 628–650. [CrossRef]
147. Jiang, Z.; Tao, W.; Yu, K.; Tan, C.; Chen, Y.; Li, L.; Li, Z. Comparative Study on Fiber Laser Welding of GH3535 Superalloy in Continuous and Pulsed Waves. *Mater. Des.* **2016**, *110*, 728–739. [CrossRef]

148. Lalehpour, A.; Barari, A. A More Accurate Analytical Formulation of Surface Roughness in Layer-Based Additive Manufacturing to Enhance the Product's Precision. *Int. J. Adv. Manuf. Technol.* **2018**, *96*, 3793–3804. [[CrossRef](#)]
149. Yampolskiy, M.; King, W.E.; Gatlin, J.; Belikovetsky, S.; Brown, A.; Skjellum, A.; Elovici, Y. Security of Additive Manufacturing: Attack Taxonomy and Survey. *Addit. Manuf.* **2018**, *21*, 431–457. [[CrossRef](#)]
150. Gao, W.; Zhang, Y.; Ramanujan, D.; Ramani, K.; Chen, Y.; Williams, C.B.; Wang, C.C.L.; Shin, Y.C.; Zhang, S.; Zavattieri, P.D. The Status, Challenges, and Future of Additive Manufacturing in Engineering. *Comput. Des.* **2015**, *69*, 65–89. [[CrossRef](#)]
151. Mahmood, M.A.; Visan, A.I.; Ristoscu, C.; Mihailescu, I.N. Artificial Neural Network Algorithms for 3D Printing. *Materials* **2021**, *14*, 163. [[CrossRef](#)]
152. Leung, C.L.A.; Marussi, S.; Atwood, R.C.; Towrie, M.; Withers, P.J.; Lee, P.D. In Situ X-Ray Imaging of Defect and Molten Pool Dynamics in Laser Additive Manufacturing. *Nat. Commun.* **2018**, *9*, 1–9. [[CrossRef](#)]
153. Lee, Y.S.; Kirka, M.M.; Ferguson, J.; Paquit, V.C. Correlations of Cracking with Scan Strategy and Build Geometry in Electron Beam Powder Bed Additive Manufacturing. *Addit. Manuf.* **2020**, *32*, 101031. [[CrossRef](#)]
154. Attallah, M.M.; Jennings, R.; Wang, X.; Carter, L.N. Additive Manufacturing of Ni-Based Superalloys: The Outstanding Issues. *MRS Bull.* **2016**, *41*, 758–764. [[CrossRef](#)]
155. Herzog, D.; Seyda, V.; Wycisk, E.; Emmelmann, C. Additive Manufacturing of Metals. *Acta Mater.* **2016**, *117*, 371–392. [[CrossRef](#)]
156. Brandl, E. *Microstructural and Mechanical Properties of Additive Manufactured Titanium (Ti-6Al-4V) Using Wire: Evaluation with Respect to Additive Processes Using Powder and Aerospace Material Specifications*; Shaker Verlag GmbH: Aachen, Germany, 2011.
157. Carlton, H.D.; Haboub, A.; Gallegos, G.F.; Parkinson, D.Y.; MacDowell, A.A. Damage Evolution and Failure Mechanisms in Additively Manufactured Stainless Steel. *Mater. Sci. Eng. A* **2016**, *651*, 406–414. [[CrossRef](#)]
158. Wycisk, E.; Solbach, A.; Siddique, S.; Herzog, D.; Walther, F.; Emmelmann, C. Effects of Defects in Laser Additive Manufactured Ti-6Al-4V on Fatigue Properties. *Phys. Procedia* **2014**, *56*, 371–378. [[CrossRef](#)]
159. Lütjering, G.; Williams, J.C. Commercially Pure (CP) Titanium and Alpha Alloys. In *Titanium*; Springer: Berlin/Heidelberg, Germany, 2003; pp. 149–175.
160. Zhang, H.; Zhou, J.; Muhammad, Y.; Tang, R.; Liu, K.; Zhu, Y.; Tong, Z. Citric Acid Modified Bentonite for Congo Red Adsorption. *Front. Mater.* **2019**, *6*, 5. [[CrossRef](#)]
161. Leuders, S.; Thöne, M.; Riemer, A.; Niendorf, T.; Tröster, T.; Richard, H.A.; Maier, H.J. On the Mechanical Behaviour of Titanium Alloy TiAl6V4 Manufactured by Selective Laser Melting: Fatigue Resistance and Crack Growth Performance. *Int. J. Fatigue* **2013**, *48*, 300–307. [[CrossRef](#)]
162. Köhnen, P.; Létang, M.; Voshage, M.; Schleifenbaum, J.H.; Haase, C. Understanding the Process-Microstructure Correlations for Tailoring the Mechanical Properties of L-PBF Produced Austenitic Advanced High Strength Steel. *Addit. Manuf.* **2019**, *30*, 100914. [[CrossRef](#)]